

1 **Seismicity characterization of oceanic earthquakes in the Mexican**  
2 **territory**

3  
4 **Quetzalcoatl Rodríguez-Pérez<sup>1,2,\*</sup>, Víctor Hugo Márquez-Ramírez<sup>2</sup>, and Francisco Ramón**  
5 **Zúñiga<sup>2</sup>**  
6

7 <sup>1</sup> Consejo Nacional de Ciencia y Tecnología, Dirección Adjunta de Desarrollo Científico, Mexico

8 <sup>2</sup> Centro de Geociencias, Universidad Nacional Autónoma de México, Juriquilla, Querétaro, Mexico

9  
10 **Correspondence:** Quetzalcoatl Rodríguez-Pérez ([quetza@geociencias.unam.mx](mailto:quetza@geociencias.unam.mx))

11 Víctor Hugo Márquez-Ramírez ([marvh@geociencias.unam.mx](mailto:marvh@geociencias.unam.mx))

12 Francisco Ramón Zúñiga ([ramon@geociencias.unam.mx](mailto:ramon@geociencias.unam.mx))

13

14

15

16

17

18

19

20

21

22

23

24

25

26

27

28

1 **Abstract.** We analyzed the seismicity of oceanic earthquakes in the Pacific oceanic regime of Mexico.  
2 We used data from the earthquake catalogs of the Mexican National Service (SSN), and the  
3 International Seismological Center (ISC) from 1967 to 2017. Events were classified into two different  
4 categories: intraplate oceanic (INT), and transform faults zone and mid-ocean ridges events (TF-MOR),  
5 respectively. For each category, we determined statistical characteristics such as magnitude frequency  
6 distributions, the aftershocks decay rate, the non-extensivity parameters, and the regional stress field.  
7 We obtained  $b$ -values of 1.17, and 0.82 for the INT, and TF-MOR events, respectively. TF-MOR  
8 events also exhibit local  $b$ -value variations in the range of 0.72 – 1.30. TF-MOR events follow a  
9 tapered Gutenberg-Richter distribution. We also obtained a  $p$ -value of 0.67 for the 1 May 1997 ( $M_w =$   
10 6.9) earthquake. By analyzing the non-extensivity parameters, we obtained similar  $q$ -values in the  
11 range of 1.39-1.60 for both types of earthquakes. On the other hand, the parameter  $a$  showed a clear  
12 differentiation, being higher for TF-MOR events than for INT events. This implies that more energy is  
13 released for TF-MOR events. Stress orientations are in agreement with geodynamical models for  
14 transform faults zone and mid-ocean ridges zones. In the case of intraplate seismicity, stresses are  
15 mostly related to a normal fault regime.

16

17

## 18 **1 Introduction**

19

20 Mid-ocean ridges and transform faults zones are two of the main morphological features of oceanic  
21 environments. Most of the oceanic earthquakes take place in areas close to the active spreading ridges  
22 where the seismogenic zone is narrow. For this reason, long ruptures are often required to produce large  
23 oceanic earthquakes. The rupture process of oceanic events is still poorly understood. Previous studies  
24 showed that these types of events have peculiar characteristics. For example, estimates of seismic

1 coupling for oceanic transform faults indicate that about three-fourths of the accumulated moment are  
2 released aseismically (Abercrombie and Ekström, 2003; Boettcher and Jordan, 2004). Early studies  
3 also showed that some oceanic events exhibit slow slip ruptures (Kanamori and Stewart, 1976; Okal  
4 and Stewart, 1992; McGuire et al., 1996). On the other hand, others proposed that the slow ruptures  
5 may be explained as numerical artifacts generated by the inversion procedures (e.g., Abercrombie and  
6 Ekström 2001; 2003). Several oceanic strike-slip events were reported as being energy deficient at  
7 high-frequencies (Beroza and Jordan, 1990; Stein and Pelayo, 1991; Ihmlé and Jordan, 1994), or  
8 having high apparent stresses (Choy and Boatwright, 1995; Choy and McGarr, 2002). On another front,  
9 oceanic earthquakes also occur as intraplate events, but to a lesser extent.

10

11 From the statistical perspective, previous studies showed that the magnitudes of the major events in the  
12 mid-oceanic ridges and transform faults zones are relatively small ( $6.0 \leq M_w \leq 7.2$ ) compared to  
13 continental events. The  $b$ -value in oceanic environments showed significant variability. For example,  
14 Tolstoy et al. (2001) reported high  $b$ -values ( $b \sim 1.5$ ) in the Gakkel Ridge associated with volcanic  
15 activity. In the Southwest Indian Ridge, Läderach (2011) found  $b$ -values of about 1.28. Bohnenstiehl et  
16 al. (2008) quantified the  $b$ -value in the East Pacific Rise, obtaining estimations in the range of  $1.10 < b$   
17  $< 2.50$ . Global studies have also shown that the mid-ocean ridge transform seismicity follows a tapered  
18 frequency-moment distribution (Kagan and Jackson, 2000; Boettcher and McGuire, 2009). Cowie et al.  
19 (1993) studied the seismic coupling on mid-ocean ridges. They found that fast-spreading ridges ( $\geq 9.0$   
20 cm/yr) are weakly coupled. On the contrary, slow-spreading ridges ( $\leq 4.0$  cm/yr) are strongly coupled  
21 (Cowie et al., 1993). For oceanic ridge transform faults, the seismic coupling coefficient ( $\chi$ ) mainly  
22 varies from 0.01 to 0.97 with an abnormal reported value of 1.79 (Table B1 of Boettcher and Jordan,  
23 2004). This unusual high value of  $\chi$  reported by Boettcher and Jordan (2004) was excluded from their  
24 analysis. The seismic coupling coefficient is in the range of  $0 \leq \chi \leq 1$ . A value of  $\chi = 1$  represents a full

1 seismic coupling. In Mexico, oceanic earthquakes have been poorly studied. There are no systematic  
2 studies on their statistical characteristics. In this article, we characterized the oceanic seismicity in  
3 Mexico. We determined the orientation of the principal stresses, the *b*- and *p*-values, and the non-  
4 extensivity parameters. The results may help to understand the ocean tectonics, particularly in Mexico.

5

## 6 **2 Tectonic Setting**

7

8 The Pacific oceanic regime of Mexico is an active area exhibiting ongoing tectonic plate interactions.  
9 These interactions involve the Cocos (CO), the Pacific (PA), the Rivera (RI), and the North American  
10 (NA) plates (Fig. 1). The Gulf of California and the Middle America Trench (MAT) are separated by  
11 the Tamayo Fracture Zone (TFZ) (Fig. 1). The convergence rate between the RI, and NA plates  
12 decreases northward along the MAT (averaging about 2–3 cm/yr in the RI plate, which is slower than  
13 the adjacent CO plate, about 5–7 cm/yr) (NUVEL-1a model, DeMets et al., 1994) (Fig. 1). Sea-floor  
14 spreading takes place along the northernmost segment of the East Pacific Rise in the Cocos, and Rivera  
15 segments (EPR-CS, and EPR-RS, respectively) (Fig. 1). In the EPR-RS, the spreading rates range from  
16 5.3 cm/year at the northern to 7.3 cm/year at the southern end of the rise (Bandy, 1992) (Fig. 1). The  
17 spreading rates at the EPR-CS are: 7.0 cm/yr near the Rivera Fracture Zone (RFZ); 8.2 cm/yr near the  
18 Orozco Fracture Zone (OFZ); 10.1 cm/yr near the Clipperton Fracture Zone (CFZ); and 10.7 cm/yr  
19 near the Siqueiros Fracture Zone (SFZ) based on the NUVEL-1a model (DeMets et al., 1994; Pockalny  
20 et al., 1997) (Fig. 1). The Rivera Transform (RT) is a left transform fault with fast slipping (~ 7.0  
21 cm/year) (Bandy et al., 2011) (Fig. 1). Due to these differences in subduction, and spreading rates, and  
22 convergence direction of the RI and CO plates, complex seismicity patterns are generated in this  
23 region. In the last century, some intermediate-size earthquakes have taken place in the Pacific oceanic  
24 regime of Mexico such as: the 14 January 1899 ( $M = 7.0$ ) (DNA project); the 17 December 1905 ( $M_w =$



1 7.0) (Pacheco and Sykes, 1992); the 10 April 1906 ( $M_w = 7.1$ ) (Pacheco and Sykes, 1992); the 31  
2 October 1909 ( $M_s = 6.9$ ) (ISC catalog); the 31 May 1910 ( $M_s = 7.0$ ) (ISC catalog); the 29 October 1911  
3 ( $M_s = 6.8$ ) (ISC catalog); the 16 November 1925 ( $M_s = 7.0$ ) (Abe, 1981); the 28 May 1936 ( $M_s = 6.8$ )  
4 (ISC catalog); the 30 June 1945 ( $M_s = 6.8$ ) (ISC catalog); the 04 December 1948 ( $M_s = 6.9$ ) (ISC  
5 catalog); the 29 September 1950 ( $M_s = 7.0$ ) (Abe, 1981); and the 1 May 1997 ( $M_w = 6.9$ ) (Global CMT  
6 catalog) earthquakes (Table 1 and Fig. 2).

7

### 8 **3 Data and Methods**

9

#### 10 **3.1 Data**

11 We used earthquake catalogs of the Mexican National Service (SSN), and the International  
12 Seismological Center (ISC) from 1967 to 2017. Events without magnitude were excluded from our  
13 analysis. Reported magnitudes (based on superficial,  $M_s$ ; body,  $m_b$ ; and coda,  $M_c$ ; waves) were  
14 converted to moment magnitude ( $M_w$ ). The SSN reports  $M_w$  for events in Mexico. For the case of the  
15 ISC events,  $M_s$ , and  $m_b$  were converted to  $M_w$  using the scaling relationships of Scordilis (2006). We  
16 classified the seismic events into two different categories: 1) intraplate oceanic events (INT, red dots in  
17 Fig. 2), and 2) transform faults zone and mid-ocean ridges events (TF-MOR, green dots in Fig. 2). The  
18 INT catalog consists of 177 events with magnitudes in the range of 2.9 - 6.0. The TF-MOR catalog is  
19 made of 2074 earthquakes with magnitudes in the following interval 2.7 - 6.9. We also used the Global  
20 CMT focal mechanism catalog (Dziewonski et al., 1981; Ekström et al., 2012) with solutions from  
21 1976 to 2017. For the stress analysis, the focal mechanism catalog was divided into 6 sub-catalogs  
22 shown in Fig. 8 (R1 to R6).

23

24

## 1 3.2 Methods

### 2 3.2.1 Moment/magnitude earthquake distributions

3 The Gutenberg-Richter law describes the occurrence of earthquakes as a function of their magnitude  
4 (Ishimoto and Iida, 1939; Gutenberg and Richter, 1944). Mathematically, this law is expressed by the  
5 following equation:  $\log_{10} N(M) = a - bM$ , where  $N(M)$  is the cumulative number of earthquakes with a  
6 magnitude larger than a given magnitude limit ( $M$ ), the constant  $b$  (or  $b$ -value) describes the slope of  
7 the size distribution and the constant  $a$  is proportional to the seismic productivity. The  $b$ -value  
8 describes the distribution of small to large earthquakes in a sample. The  $b$ -value is considered to be a  
9 feature for a given tectonic environment (e.g., Scholz, 1968; Wyss, 1973; Smith, 1981; Wiemer and  
10 Benoit, 1996). In several tectonic environments,  $b$  is close to 1 (Utsu, 1961), but many factors affect it.  
11 Among them, high thermal gradients and rock heterogeneity (Mogi, 1962; Warren and Latham, 1970)  
12 increases the  $b$ -values. On the contrary, increments in effective and shear stresses (Scholz, 1968; Wyss,  
13 1973; Urbancic et al., 1992) reduce the  $b$ -value. The  $b$ -value differs between unrelated fault zones  
14 (Wesnousky, 1994; Schorlemmer et al., 2005), but also for specific space and time periods (Nuannin et  
15 al., 2012). Schorlemmer et al. (2005) found a global dependence of the  $b$ -value on focal mechanism,  
16 which was corroborated at a regional level by Rodríguez-Pérez and Zúñiga (2018). According to those  
17 authors, the highest  $b$ -values correspond to normal-faulting events, followed by strike-slip, and thrust  
18 earthquakes, respectively. We estimated the  $b$ -value by the maximum likelihood formula of Aki (1965),  
19 and the completeness magnitude ( $M_c$ ) with the maximum curvature method (Wiemer and Wyss, 2000).  
20 We used the ZMAP software package (Wiemer, 2001) for estimating the  $b$ -value, and  $M_c$ .

21

22 As reported by previous authors, seismicity on the mid-ocean transform faults is better represented by a  
23 tapered frequency moment distribution (e.g., Boettcher and McGuire, 2009). This distribution has the  
24 following form (Kagan, 1997, 1999; Kagan and Jackson, 2000; Kagan and Schoenberg, 2001; Vere-

1 Jones et al., 2001):

2

$$3 \quad N(M) = N_0 \left( \frac{M_0}{M} \right)^\beta \exp \left( - \frac{M_0 - M}{M_m} \right), \quad (1)$$

4

5 where  $\beta$  is one of the parameters to determine ( $\beta = (2/3)b$ , where  $b$  is the  $b$ -value),  $N_0$  is the cumulative  
6 earthquake number over a completeness threshold seismic moment ( $M_0$ ), and  $M_m$  is the maximum  
7 expected moment. We analyzed if this frequency distribution is suitable for describing the seismicity of  
8 oceanic events in Mexico. In order to calculate the tapered Gutenberg-Richter distribution, we used the  
9 Matlab function `Get_GR_parameters.m` developed by Olive (2016). The tapered Gutenberg-Richter  
10 moment distribution is fitted by means of a least-squares inversion following Frohlich (2007).

11

### 12 **3.2.2 Temporal distribution of aftershocks**

13 The frequency distribution of the decrement of earthquake aftershocks is described by the modified  
14 Omori's law (Utsu, 1961; Utsu et al., 1995) as:

15

$$16 \quad R(t) = \frac{k}{(t+c)^p}, \quad (2)$$

17

18 where  $R(t)$  is the rate of occurrence of aftershocks within a given magnitude range,  $t$  is the time interval  
19 from the mainshock,  $k$  is the productivity of the aftershock sequence,  $p$  is the power-law exponent ( $p$ -  
20 value), and  $c$  is the time delay before the onset of the power-law aftershock decay rate. Variations of  $p$ -  
21 values exist for different tectonic regimes, and each aftershock sequence. As before, we used the  
22 ZMAP software package (Wiemer, 2001) for estimating the  $p$ -value of the aftershock sequence of the 1

1 May 1997 earthquake ( $M_w = 6.9$ ).

2

### 3 **3.2.3 Fragment-asperity model**

4 Sotolongo-Costa and Posadas (2004) introduced ~~the~~ fragment-asperity model to describe the  
5 earthquake dynamics in a Tsallis entropy non-extensive framework (Tsallis, 1988). This model takes  
6 into consideration the irregular surfaces of two fault planes in contact and the rock fragments of  
7 different shape and sizes that fill the space between them. According to this model, earthquakes are  
8 triggered by the interaction along the fault planes of these rock fragments. Considering that large  
9 fragments are more difficult to release than small ones, the resulting energy is assumed to be  
10 proportional to the volume of the fragment (Telesca, 2010). Silva et al. (2006) improved the model and  
11 found a scaling law between the released energy ( $\epsilon$ ), and the size of asperity fragments ( $r$ ) by the  
12 following proportional factor:  $\epsilon \propto r^3$ . The non-extensive statistics is used to describe the volumetric  
13 distribution function of the fragments. A parameter that represents the proportion between  $\epsilon$  and  $r$  is  
14 introduced. This parameter is known as the  $a$ -value or parameter  $a$  (Silva et al., 2006; Telesca, 2010).  
15 The parameter  $a$  is defined using a volumetric distribution function of the fragments applying the  
16 maximum entropy principle for the Tsallis entropy (for details in the mathematical expressions see  
17 Silva et al., 2006; Telesca, 2010). The magnitude cumulative distribution function becomes:

18

$$19 \quad \log_{10}(N>M) = \log_{10}(N) + \left(\frac{2-q}{1-q}\right) \log_{10} \left[ 1 - \left(\frac{1-q}{2-q}\right) \left(\frac{10^K}{a^{2/3}}\right) \right], \quad (3)$$

20

21 where  $N$  is the total number of earthquakes;  $N (>M)$  represents the number of events with magnitude  
22 larger than  $M$ ;  $a$  is a proportionality parameter between  $\epsilon$  and  $r$ , and;  $q$  is the non-extensivity parameter.

23  $K$  is defined as  $K = 2M$  (Silva et al., 2006), or  $K = M$  (Telesca, 2011). The magnitude ( $M$ ) is related to

1  $\epsilon$  by the following relation:  $M = 1/3 \log(\epsilon)$  (Silva et al., 2006). Telesca (2011) considered that the  
2 relation between  $\epsilon$  and  $M$  is given by  $M = 2/3 \log(\epsilon)$  (Telesca, 2011). None of both models are preferred  
3 over the other. We used both models in order to quantify the variability of the non-extensive  
4 parameters. According to Telesca (2010), the physical meaning of the  $q$ -parameter consists in that it  
5 provides information about the scale of interactions. It means that if  $q$  is close to 1, the physical state is  
6 close to the equilibrium. As a result, few earthquakes are expected. On the other hand, as  $q$  rises, the  
7 physical state goes away from the equilibrium state, this implies that the fault planes are able to  
8 generate more earthquakes, thus resulting in an increment in the seismic activity (Telesca, 2009; 2011).  
9 The physical meaning of the  $a$ -value lies in the fact that it provides a measure of the energy density. It  
10 means that the  $a$ -value is large if the energy released is large (Telesca, 2011). For example, high  $a$ -  
11 values are expected when the events with the highest magnitude take place. Previous studies have  
12 shown that the  $q$ -value ranges mainly from 1.50 to 1.70 (Vilar et al., 2007; Vallianatos, 2009;  
13 Rodríguez-Pérez and Zúñiga, 2017; among others). We obtained the  $a$  and  $q$  parameters by minimizing  
14 the root mean square error (RMS) with the Nelder-Mead method (Nelder and Mead, 1965).

15

### 16 3.2.5 Stress Inversion

17 In order to study the regional stress field for oceanic earthquakes, we performed stress tensor inversion  
18 from focal mechanisms reported in the Global CMT catalog (Dziewonski et al., 1981; Ekström et al.,  
19 2012) with the iterative joint inversion developed by Vavryčuk (2014). From the stress inversion, we  
20 obtained the orientation of the principal stress axes  $\sigma_1$ ,  $\sigma_2$ , and  $\sigma_3$  (where  $\sigma_1 \geq \sigma_2 \geq \sigma_3$ ), and the stress  
21 ratio  $R$ . We now briefly explain each method. The first method (the iterative joint inversion), provides  
22 an accurate estimation of  $R$  and stress orientations (Vavryčuk, 2014). In this method, the ratio is defined  
23 as  $R = (\sigma_1 - \sigma_2) / (\sigma_1 - \sigma_3)$  (Gephart and Forsyth, 1984). A fault instability constraint is applied, and the  
24 fault is identified with that nodal plane which is more unstable, and thus more susceptible to faulting

1 (Vavryčuk, 2014). By incorporating a fault instability constraint into the inversion, an iterative  
2 procedure is imposed. The uncertainties are determined as the differences between the inverted results  
3 considering noisy data (Vavryčuk, 2014). The stress inversion was carried out with the  
4 STRESSINVERSE software developed by Vavryčuk (2014). The maximum horizontal stress ( $SH_{max}$ )  
5 was calculated using the formulation of Lund and Townend (2007). The stress inversion was performed  
6 for each of the six different regions shown in Fig. 7.

7

#### 8 **4 Results**

9

10 The  $b$ -value for the INT events is  $1.17 \pm 0.1$  with a  $M_c = 4.4$  (Fig. 3). The cumulative seismic moment  
11 for these events is  $\sum M_0 = 3.57 \times 10^{25}$  Nm. For the INT events, the non-extensive parameters are:  $q =$   
12  $1.60$ , and  $a = 6.69 \times 10^{12}$ ; and  $q = 1.39$ , and  $a = 2.27 \times 10^6$  for the Silva's and Telesca's models,  
13 respectively (Fig. 3). For INT events, both models have similar curve fittings (Fig. 3). In the case of the  
14 TF-MOR events, the  $b$ -value is  $0.82 \pm 0.02$  with a  $M_c = 4.2$  (Fig. 4a). The cumulative seismic moment  
15 for these events is  $\sum M_0 = 12.76 \times 10^{26}$  Nm. TF-MOR events also exhibit local  $b$ -value variations in the  
16 range of  $0.72 - 1.30$  (Fig. 4b) for each of the subregions R1 to R5 (Table 2). Results for TF-MOR  
17 events also show that the tapered Gutenberg-Richter distribution fits better the earthquake data than the  
18 common Gutenberg-Richter distribution (Fig. 5a). The tapered Gutenberg-Richter distribution was  
19 fitted with the following parameters:  $\beta = 0.64$ , and the estimated magnitude of  $M_m = 6.7$  (Fig. 5a). The  
20 regions that have the worst fitting with a Gutenberg-Richter distribution are subregions R1 and R2  
21 (Figs. 4b and 5b). In the case of the TF-MOR events, the non-extensive parameters are:  $q = 1.60$ , and  $a$   
22  $= 3.22 \times 10^{13}$ ; and  $q = 1.41$ , and  $a = 3.55 \times 10^6$  for the Silva's and Telesca's models, respectively (Fig. 6).  
23 TF-MOR events also exhibit local  $a$  and  $q$ -value variations for each of the subregions R1 to R5 (Table  
24 2, and Fig. 6). For TF-MOR events, the best fit was obtained with Telesca's model (Fig. 6). By

1 analyzing the aftershock sequence of the 1 May 1997 earthquake ( $M_w = 6.9$ ), we found a  $p$ -value of  
2  $0.67 \pm 0.33$  (Table 3). The magnitude of the largest aftershock of the 1997 event is  $M_w = 5.3$  (Table 3).

3  
4 The region R1 is composed of strike-slip (70.3%), strike-slip with normal and reverse components  
5 (21.6%, and 5.4%, respectively), and normal-faulting (2.7%) focal mechanisms (Fig. 7b). In region R2,  
6 there are strike-slip (82.4%), and strike-slip with normal and reverse components earthquakes (9.5 %,  
7 and 8.1 %, respectively) (Fig. 7b). Region R3 is composed of strike-slip (62.5%), strike-slip with  
8 normal component (25%), normal-faulting with strike-slip component (6.3%), and reverse events  
9 (6.3%)(Fig. 7b). In region R4, there are strike-slip (70.8%), strike-slip with normal and reverse  
10 components (8.3%, and 16.7 %, respectively), and reverse events (4.2%)(Fig. 7b). In region R5, strike-  
11 slip (53%), strike-slip with normal and reverse components(23.5%, and 17.6%, respectively), and  
12 reverse (5.9%) earthquakes take place (Fig. 7b). For the case of region R6, earthquakes exhibit a  
13 normal (83.3%) and normal-faulting with strike-slip component (16.7%) focal mechanisms (Fig. 7b).

14  
15 Table 4 summarizes the results from the stress inversion. The region R6 is only dominated by N and N-  
16 SS earthquakes (Fig. 8). In regions R4 and R5, stress results showed moderate similarities. The  
17 differences in these regions may also be related to the variability of the focal mechanisms (here we  
18 have SS, SS-N, SS-R, and to lesser extent R events) (Fig. 8). Variations are very significant in regions  
19 R1 to R3 (spatially in  $\sigma_2$ ) (Table 4). These regions also showed different types of events: SS, SS-N, SS-  
20 R for R1; SS, SS-N, SS-R for R2; and SS, SS-N, N-SS, R for R3 (Fig. 8). In the case of the East Pacific  
21 Rise Rivera segment (region R1),  $\sigma_2$  is almost vertical, and  $SH_{\max}$  is  $\sim 170^\circ$  suggesting a strike-slip  
22 regime (Table 4). For the case of the Rivera Transform (region R2),  $\sigma_2$  is quasi vertical, and the  $SH_{\max}$  is  
23  $157^\circ$  suggesting a strike-slip regime (Table 4). In region R3,  $\sigma_2$  is almost vertical, and the  $SH_{\max}$  is also  
24  $157^\circ$  suggesting a strike-slip regime (Table 4). For the region R4,  $\sigma_2$  is  $76^\circ$ , and the  $SH_{\max}$  is  $22^\circ$

1 suggesting a strike-slip regime (Table 4). In R5,  $\sigma_2$  is from  $69^\circ$ , and the  $SH_{\max}$  is  $120^\circ$  suggesting a  
2 strike-slip regime (Table 4). In R6, the principal axes are related to a normal fault regime.  $\sigma_1$  is almost  
3 vertical, and the  $SH_{\max}$  is  $\sim 45^\circ$  (Table 4).

4

## 5 **Discussion**

6

7 One of the main problems for studying oceanic seismicity is that the epicenters are located far from  
8 most of the recording stations in mainland Mexico. This has a direct effect on the earthquake  
9 magnitude distributions ( $M_c$  and  $b$ -value). Our results show that  $M_c$  is 4.4 and 4.2 for INT and TF-MOR  
10 events, respectively.  $M_c$  for oceanic events is higher than reported  $M_c$  for the subduction zone, and  
11 continental regions of Mexico. The magnitude completeness for oceanic earthquakes differs for  
12 different ~~parts of the World~~, but in most cases it is in the range of 4.0 – 5.0 on average ~~considering most~~  
13 ~~of the global catalogs~~. Several microseismic surveys have been conducted in different oceanic  
14 environments (e.g., Smith et al., 2003; Simão et al., 2010; McGuire et al., 2012; among others). As a  
15 result of these studies, precise hypocenter locations and earthquake distributions with a broader  
16 magnitude range were obtained. Thus lower  $M_c$  is reported for studies based on microseismic surveys.  
17 For example, in the Mid-Atlantic Ridge,  $M_c \sim 3.0$  with several smaller events ( $M_w < 2.5$ ) were reported  
18 (Bohnenstiehl et al., 2002; Smith et al., 2002, and 2003).

19

20 The location uncertainty plays an important role when earthquakes are assigned to an intraplate or a  
21 mid-ocean ridge/transform fault environment. For example, some studies reported that for faults  
22 located at 4S on the EPR, teleseismic locations could be off as much as 50 km (McGuire, 2008;  
23 Wolfson-Schwehr, 2014). As a consequence, some TF-MOR events are probably classified as INT  
24 events, and vice-versa (for example, epicenters in color in Fig. 2). Some events located in the Tamayo



1 Fracture Zone close to the Rivera subduction zone may also be mislabeled. This mislocation effect  
2 introduces uncertainties on the estimation of the statistical parameters. In order to have precise  
3 locations an avoid mislocation, ocean-bottom seismometers along the Mexican coast are needed. Being  
4 aware of this, one should avoid over-interpretation of the results. Local monitoring of oceanic events  
5 represents an improvement of more than an order of magnitude relative to the regional, and teleseismic  
6 detection levels. For this reason, it is difficult to establish a direct comparison with our results with  
7 those from studies based on microseismic surveys.

8

9 Previous studies also showed that the seismicity on oceanic transform faults that connect mid-ocean  
10 ridges are thermally controlled (Abercrombie and Ekström, 2001; Boettcher et al., 2007). Regarding  
11 the thermal effect on the seismogenic zone. It is essential to mention that faults along the middle and  
12 southern segments of the EPR are shorter and faster-slipping. The faster slip rates and shorter fault  
13 lengths result in narrower seismogenic zones because the thermal structure is shallow. On the other  
14 hand, the Rivera Transform is longer, and has a slower slip rate, resulting in a wider seismogenic zone.  
15 However, heat is not the only factor that regulates seismicity because the largest events break a small  
16 part of the rupture areas predicted by thermal models (Boettcher and Jordan, 2004; Roland et al., 2010).  
17 Thus most slip occurs without producing large earthquakes (Boettcher and Jordan, 2004; Roland et al.,  
18 2010). This can explain the occurrence of a few events with  $M > 6.5$  in the Rivera Transform.  
19 According to McGuire et al. (2012), the apparent lack of large events on mid-ocean ridge transform  
20 faults may also be related to the heterogeneity of materials on the fault plane. The maximum magnitude  
21 for transform fault events on the East Pacific Rise (in the latitude interval of  $3^\circ < \text{Lat} < 5^\circ$ ) is about 6.5  
22 (McGuire et al., 2005). On the other hand, earthquakes in the Rivera Transform and on the northern  
23 segment of the East Pacific Rise (in Mexico) have relative larger magnitudes ( $M > 6.8$ ) based on  
24 reported seismicity in different catalogs (Fig. 1). This highlights a differentiation between the mid-and

1 southern and northern segments of the East Pacific Rise.

2

3 Earthquake statistical studies showed that large oceanic events in transform faults, fracture zones, and  
4 intraplate regions release low energy levels in their aftershock sequences (Houston et al., 1993;  
5 Boettcher and Jordan, 2001; Antolik et al., 2006). Boettcher et al. (2012) found that earthquakes on  
6 transform faults have an order of magnitude fewer aftershocks than intraplate events. According to  
7 some authors, a low aftershock-to-mainshock energy ratio indicates an efficient rupture or complete  
8 stress drop in the mainshock presupposing a weak fault (Hwang and Kanamori, 1992; Velasco et al.,  
9 2000). Many factors can affect the aftershock productivity, for example the age of the lithosphere and  
10 the heat flux have a direct influence on the rock strength (Antolik et al., 2006), thus, explaining the low  
11 energy release in the aftershock sequence of oceanic events. The observed low aftershock energy seems  
12 to be a common feature of oceanic earthquakes (Antolik et al., 2006). In this regard, we studied the 1  
13 May 1997 ( $M_w = 6.9$ ) strike-slip event in the Rivera Transform and its largest aftershock ( $M_w = 5.3$ ). By  
14 considering the energy magnitude as  $\log E = 1.5 M_w + 11.8$ , we obtain that the energy of the mainshock  
15 is  $1.41 \times 10^{22}$  ergs, and the energy of the largest aftershock is  $5.62 \times 10^{19}$  ergs resulting in an aftershock-  
16 to-mainshock energy ratio of 0.003. This value is considered as low and representative of strike-slip  
17 events, as shown by the comparison with the results reported by Velasco et al. (2000). A similar  
18 analysis comes from Båth's law by considering the magnitude difference between the mainshock, and  
19 the largest aftershock. We determined that the magnitude difference for the 1997 event is 1.6, which is  
20 higher than the theoretical value of 1.2. Both magnitude difference and the aftershock-to-mainshock  
21 energy ratio showed large scatter (e.g., Velasco et al., 2000; Utsu, 2002), and results ought to be taken  
22 with caution.

23

24 The aftershock decay rate is the product of the strain relaxation around the rupture plane. Aftershock

1 studies have shown that oceanic ridges are prone to have  $p$ -values greater than one due to the high  
2 temperature of the oceanic crust resulting in rapid strain release (Kisslinger, 1996; Rabinowitz and  
3 Steinberg, 1998; Klein et al., 2006). According to previous studies, extremely high  $p$ -values ( $p > 2$ ),  
4 and short aftershock durations are related to high temperatures (Bohnenstiehl et al., 2002; Simão et al.,  
5 2010), and/or migration of hydrothermal fluids (Goslin et al., 2005). Oceanic strike-slip events seem to  
6 have lower  $p$ -values than mid-ocean ridges events. For example, Bohnenstiehl et al. (2004) found a  $p$ -  
7 value of 0.95 for the 15 July 2003 ( $M_w = 7.6$ ) central Indian Ridge strike-slip event. For the Siqueiros,  
8 Discovery, and western Blanco transforms, the  $p$ -value varies from 0.94 to 1.29 (Bohnenstiehl et al.,  
9 2002). Davis and Frohlich (1991) determined a  $p$ -value of  $0.928 \pm 0.024$  for the combined ridge and  
10 transform environments. We found a  $p$ -value of  $0.67 \pm 0.33$  for the 1 May 1997 ( $M_w = 6.9$ ) strike-slip  
11 event in the Rivera transform. Our results fall within the range of global studies that showed that the  $p$ -  
12 value varies from 0.6 – 2.5 (Utsu et al., 1995). We also reported a  $c$  close to 0 for the aftershock  
13 sequence of the 1 May 1997 ( $M_w = 6.9$ ) (Table 3). Shcherbakov et al. (2004) found that the parameter  $c$   
14 of the Omori's law decreases as the magnitude of events considered increases. According to them, this  
15 observation is due to the effect of an undercount of small aftershocks in short time periods. This  
16 provides an explanation for our result of  $c \sim 0$  because of the limited magnitude detection reported in  
17 the regional and global catalogs used.

18

19 Estimations of  $b$ -value at different scales (local, regional, or global) have shown a significant departure  
20 from the theoretical result of  $b \sim 1$ . In the case of the oceanic events, previous studies showed large  
21 fluctuations in the  $b$ -values. For example, Tolstoy et al. (2001) reported  $b$ -values of about 1.5  
22 associated with volcanic activity in the Gakkel Ridge. Läderach (2011) reported  $b$ -values of 1.28 in the  
23 Southwest Indian Ridge. In a global study, Molchan et al. (1997) estimated the  $b$ -value for mid-ocean,  
24 and transform zones, obtaining values of the following interval 0.97 – 1.47. Along the East Pacific Rise

1 (in the latitude interval of  $5^{\circ}\text{N} < \text{Lat} < 9.90^{\circ}\text{N}$ ),  $b$ -value fluctuates from 1.10 to 2.50 (Bohnenstiehl et  
2 al., 2008). Bohnenstiehl et al. (2008) determined the  $b$ -value of 9000 earthquakes with magnitudes in  
3 the range of  $-1.5 - 1.0$ . The study of Bohnenstiehl et al. (2008) took place in the southern part of our  
4 study zone, but their results are based on microearthquakes occurring in 1 year. Due to this overlap, we  
5 compare their results with our results for region R5. For R5, we obtained a  $b$ -value of 0.94 with a  $M_c$  of  
6 4.2. Bohnenstiehl et al. (2008) found that the  $b$ -value approaches 2.5 at very shallow depths ( $< 0.3$  km)  
7 (with  $M_c = -1.3$ ). At depths of 0.5 to 1.5 km, the  $b$ -values drops to a value of 1.10 (with  $M_c = -0.4$ ).  
8 According to Bohnenstiehl et al. (2008) at very shallow depths, the uppermost oceanic crust is  
9 structurally heterogeneous because of the extrusion of lava, and the repeated emplacement of sheeted  
10 dikes. As a consequence, there is a large proportion of small versus large earthquakes resulting in high  
11  $b$ -values. The  $b$ -values decreases with depth due to the decreasing heterogeneity, and/or changes in  
12 ambient stress levels. Considering that events in our catalog for R5 occur at a different depth interval,  
13 and assuming the decreasing heterogeneity, less low magnitude events are expected (reducing the  $b$ -  
14 value). Another explanation for the differences between our results and the results of Bohnenstiehl et  
15 al. (2008) is that the magnitude ranges of the earthquake catalogs are extremely different. This  
16 highlights how the  $b$ -value is affected by magnitude completeness.

17

18 Statistical studies suggested that  $\beta$ -value mainly takes values between 0.60 and 0.70 for a global range  
19 (Kagan, 2002). Bird et al. (2002) studied the tapered Gutenberg-Richter distribution for spreading  
20 ridges and oceanic transform faults based on global data obtaining a  $\beta$ -value of about 0.67 for both  
21 types of events. Bird et al. (2002) reported corner magnitudes ( $M_m$  in Eq. (1)) varies from 5.8 to 6.6 –  
22 7.1 for mid-ocean ridge and transform faults, respectively. Bird et al. (2002) also found a dependence  
23 of  $\beta$ -value on the relative plate velocity. According to them, the  $\beta$ -value is higher (with  $M_m = 7.1$ ) when  
24 the velocity is  $< 36$  mm/yr than when the velocity is  $> 67$  mm/yr (with  $M_m = 6.6$ ) for spreading ridges,

1 and oceanic transform faults, respectively. These observations are in agreement with our estimate of  $\beta =$   
2 0.64, and  $M_m$  of 6.6 for oceanic earthquakes in Mexico (Figure 5). For intraplate events, we obtained a  
3  $\beta > 0.70$ . According to Kagan (2010),  $\beta$ -values  $> 0.70$  may be related to the mix of earthquake  
4 populations with different maximum magnitudes ( $M_m$ ). In the case of intraplate events, we associated  
5 the somewhat high  $\beta$ -values with the mix of some intraplate, and mid-ocean- transform events. This  
6 could be related to incorrect hypocenter locations due to the difficulty of precisely locating oceanic  
7 events by the landbased networks.

8

9 The seismicity models based on non-extensivity consider the interaction of two irregular fault surfaces  
10 (asperities), and rock fragments filling them. However, these models differ in their assumption of how  
11 energy is stored in the fragments, and the asperities. This difference is expressed through the constant  
12  $a$ , which represents the proportionality between the released energy  $E$ , and the fragment size  $r$ . This  
13 explains the difference in  $a$  parameter between Telesca's and Silva's models (Fig. 5). Both models  
14 showed that  $a$  for TF-MOR is higher than  $a$  for the INT events (Fig. 5). This implies that more energy  
15 is released for TF-MOR earthquakes. On the other hand, the  $q$ -value indicates if the physical state of a  
16 seismic area moves away from equilibrium. The physical state is at equilibrium when  $q$  is equal to 1,  
17 and as  $q$  increases, the system is in an instability state in which a more significant amount of seismic  
18 energy is released. Individually, we found higher  $q$ -values for TF-MOR events than for INT events  
19 (Fig. 5), meaning that TF-MOR events are farther from the equilibrium than INT events. The results  
20 showed a better fitting for cumulative distribution functions using the Telesca model for TF-MOR and  
21 each of the regions (Fig. 6). In regions R1-R5, our results showed that  $q$  varies from 1.31 to 1.52, and  
22 from 1.57 to 1.63 using the Telesca's and Silva's models, respectively. In the case of subduction zones,  
23 the  $q$ -value can vary from 1.35 to 1.70. For example, in the Hellenic Subduction Zone,  $q$  is in the range  
24 of 1.35 - 1.55 (Papadakis et al., 2013); in the Mexican subduction zone, Valverde-Esparza et al. (2012)

1 found that  $q$  varies from 1.63 to 1.70. Thus, our results conform to values obtained in regional studies.  
2  
3 Focal mechanisms provide useful information about the structure, and settings of faults, and can  
4 describe the crustal stress field in which earthquakes take place. Our analysis is limited because we  
5 only used focal mechanisms based on teleseismic data. Reported focal mechanisms confirm Sykes's  
6 model for mid-ocean ridges (Sykes, 1967), where events in transform zones tend to have strike-slip  
7 mechanisms, while ridge crest events have mainly normal faults. The teleseismic detection threshold  
8 for oceanic events in the East Pacific Rise is dependent on the region of the EPR. For example,  
9 Riedesel et al. (1982) report a magnitude detection threshold in the range of 4.0 – 5.0. For the  
10 Quebrada, Discovery, and Gofar faults, the CMT catalog is only complete to  $M_w = 5.4$ . (McGuire,  
11 2008; Wolfson-Schwehr et al., 2014). Another limitation of our study is that we combine different types  
12 of earthquakes into a single region, resulting in inaccurate estimations of the stress state for that  
13 specific region. Under these circumstances, our study provides information on the stress field of major  
14 structures or the stress associated with the dominant types of earthquake.

15  
16 In oceanic environments, the largest magnitude events along transform fault or intraplate earthquakes  
17 usually show strike-slip mechanisms (Wiens and Stein, 1984; Kawasaki et al., 1985). In the adjacent  
18 areas to the oceanic ridges where the oceanic lithosphere is young, Wiens and Stein (1984) report a  
19 large variety of focal mechanisms and stress orientations. For example, in the East Pacific Rise, in the  
20 Mexican territory, Wiens and Stein (1984) reported thrust and normal mechanism solutions for near  
21 ridge intraplate seismicity. This explains the strike-slip with normal components, as well as thrust  
22 events in regions R3, R4, and R5 (Fig. 7). In R3, and R4 (Fig. 7), the maximum horizontal axes  
23 (compression) of thrust events show a preferred orientation perpendicular to the spreading direction.  
24 On the other hand, in region R5 (Fig. 7), the compression axes, showed a weak preferred alignment

1 with respect to the spreading direction. In the Rivera transform, focal mechanisms showed right lateral  
2 strike-slip motion implying oblique horizontal stresses (Fig. 7). Although most of the events in the  
3 Rivera transform (R2 in Fig. 7) are strike-slip events, some events with unusual mechanisms have been  
4 reported (normal faulting events) (Wolfe et al., 1993). Normal faulting events may be related to  
5 extensional offsets or internal deformation of the Rivera plate (Wolfe et al., 1993).

6

## 7 **6 Conclusions**

8

9 We analyzed the seismicity of oceanic events in the Pacific oceanic regime of Mexico. Oceanic  
10 earthquakes were classified into two different categories: intraplate oceanic (INT), and transform faults  
11 zone and mid-ocean ridges events (TF-MOR), respectively. We conducted a stress state estimation for  
12 the different regions. Because of combination of different types of earthquakes into the regions, our  
13 results only provide information on the stress field of major structures or the stress associated with the  
14 dominant types of earthquakes. It is important to be aware of this limitation in order to avoid an over-  
15 interpretation of the results. TF-MOR events have strike-slip, strike-slip with normal and reverse  
16 components, normal and normal-faulting with strike-slip component, and reverse focal mechanisms.  
17 On the other hand, INT events have only normal, and normal-faulting with strike-slip component focal  
18 mechanisms. The stress field from INT, and TF-MOR events agree with global studies. Regarding the  
19 aftershock productivity, we found that the aftershock decay rate of the 1 May 1997 ( $M_w = 6.9$ ) strike-  
20 slip event in the Rivera transform is also consistent with oceanic  $p$ -value estimations. Although the  
21 limitation of the catalogs used, our results provided a general insight into the seismicity of oceanic  
22 environments. The main problem is the location uncertainty and mislabelling of the earthquakes. The  $b$ -  
23 value for INT events (1.17) is higher than that for TF-MOR events (0.82). Our  $b$ -values estimations are  
24 in agreement with other regional studies but differ from  $b$ -value estimates based on microseismicity

1 studies. Our  $b$ -value estimates for mid-ocean ridge/transform fault environments are lower ( $0.72 < b <$   
2  $1.30$ ) than those derived from microseismicity studies ( $1.1 < b < 2.5$ ). Our results also showed that TF-  
3 MOR events mostly follow a tapered Gutenberg-Richter distribution.

4

5 From the non-extensivity analysis, we observed that TF-MOR events are farther from the equilibrium  
6 than INT events. Thus high  $q$ -values take place in mid-ocean ridges, and transform faults zones. This  
7 means that mid-ocean ridge and transform faults are able to produce more seismicity. Low  $q$ -values are  
8 also reported during relatively quiet periods, characterized mainly by the occurrence of small  
9 magnitude events. This can be an explanation for the low  $q$ -values of regions R1 and R5. Our results  
10 also showed that  $a$ -values are higher for TF-MOR events than for INT events using both models. This  
11 implies that more earthquakes with larger magnitude occur (or more energy is released) in mid-ocean  
12 ridge/transform fault environments than in an oceanic continental environment. Telesca's model fits  
13 better with the cumulative magnitude distribution functions making a better option to study the oceanic  
14 seismicity in Mexico.

15

16

17

18



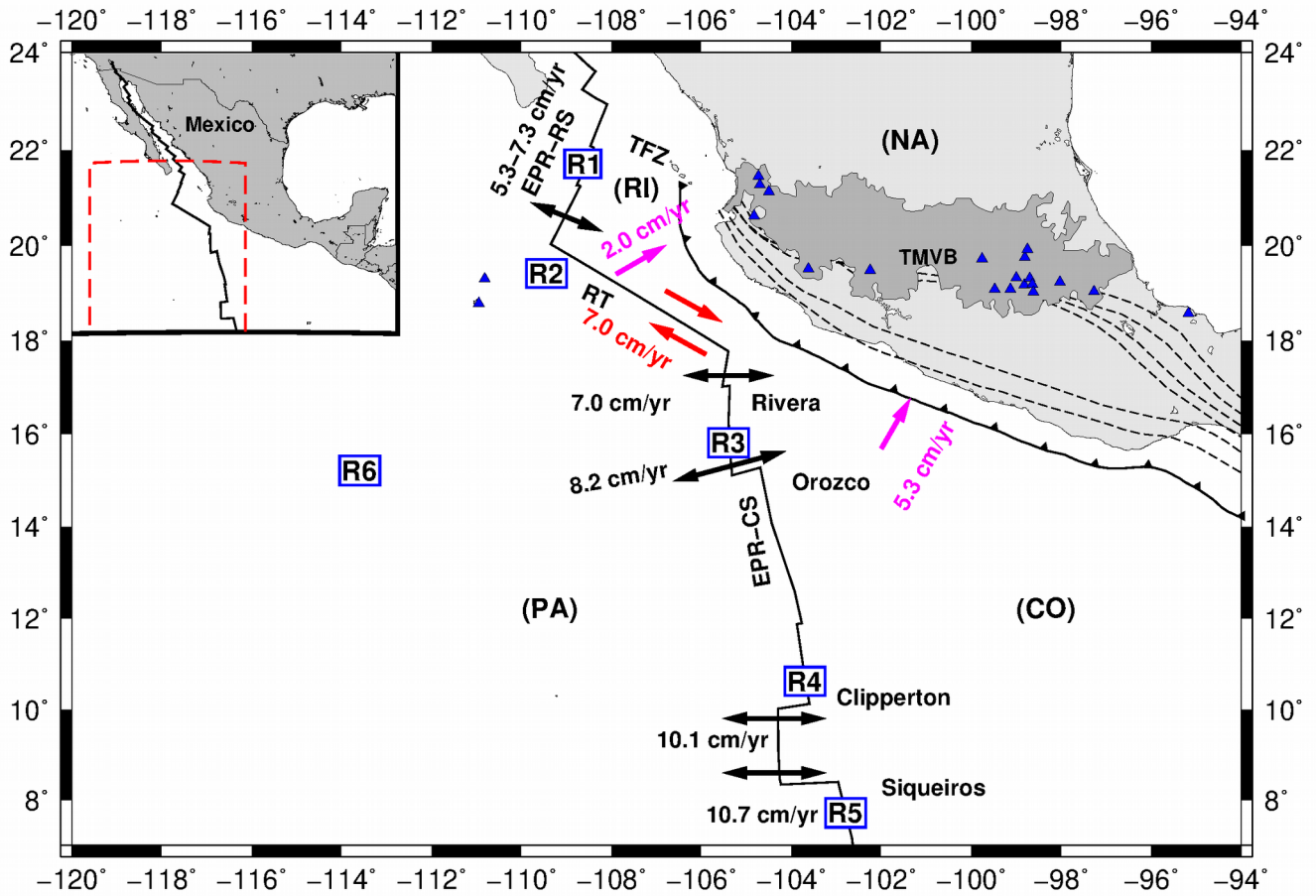


Figure 1

1  
2  
3 Main tectonic features in the Mexican territory. CO is the Cocos plate, NA is the North American plate,  
4 PA is the Pacific plate, RI is the Rivera microplate, TMVB is the Trans-Mexican Volcanic Belt, TFZ is  
5 the Tamayo fracture zone, EPR-RS is the East Pacific Rise Rivera segment, EPS-CS is the East Pacific  
6 Rise Cocos segment, and RT is the Rivera Transform. Blue triangles are volcanoes. Dashed lines show  
7 contour lines of the subducted slab. Arrows indicate the motion of the PA, CO, and RI plates. R1 to R6  
8 are the regions in which the study are were divided for analyzing stress and seismicity characteristics.  
9 Red number indicates the slipping rates. Pink numbers indicate convergence rates, and black numbers  
10 indicate spreading rates.

11  
12  
13

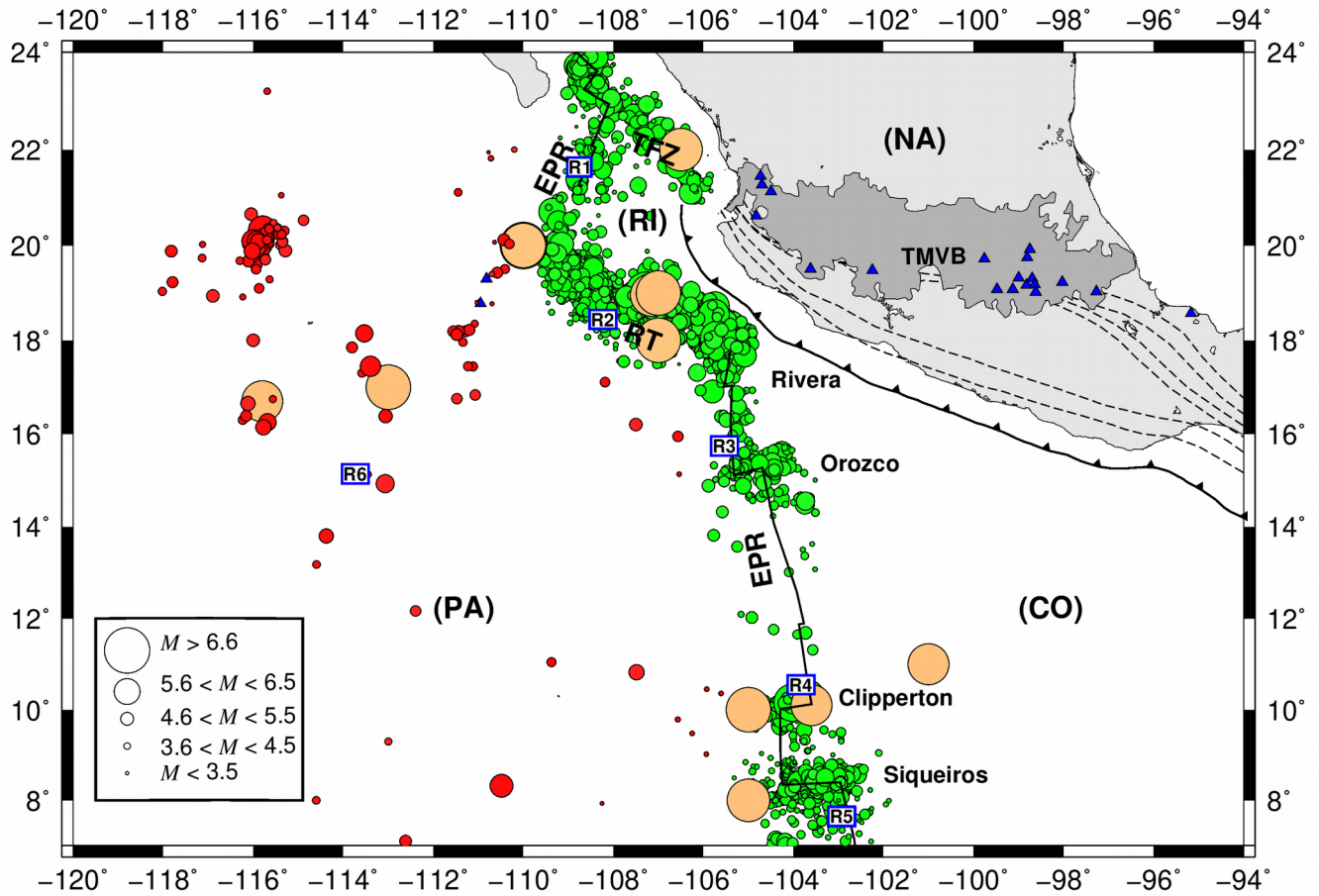


Figure 2

Oceanic seismicity in the Mexico from 1899 to 2017. The size of the circles represents magnitude. Brown circles are relevant historical earthquakes shown in Table 1 with  $M > 6.8$ . Red circles are intraplate oceanic events, and green circles are transform faults zone, and mid-ocean ridges earthquakes. Epicenters are taken from the Mexican National Service (SSN), and the International Seismological Center (ISC).

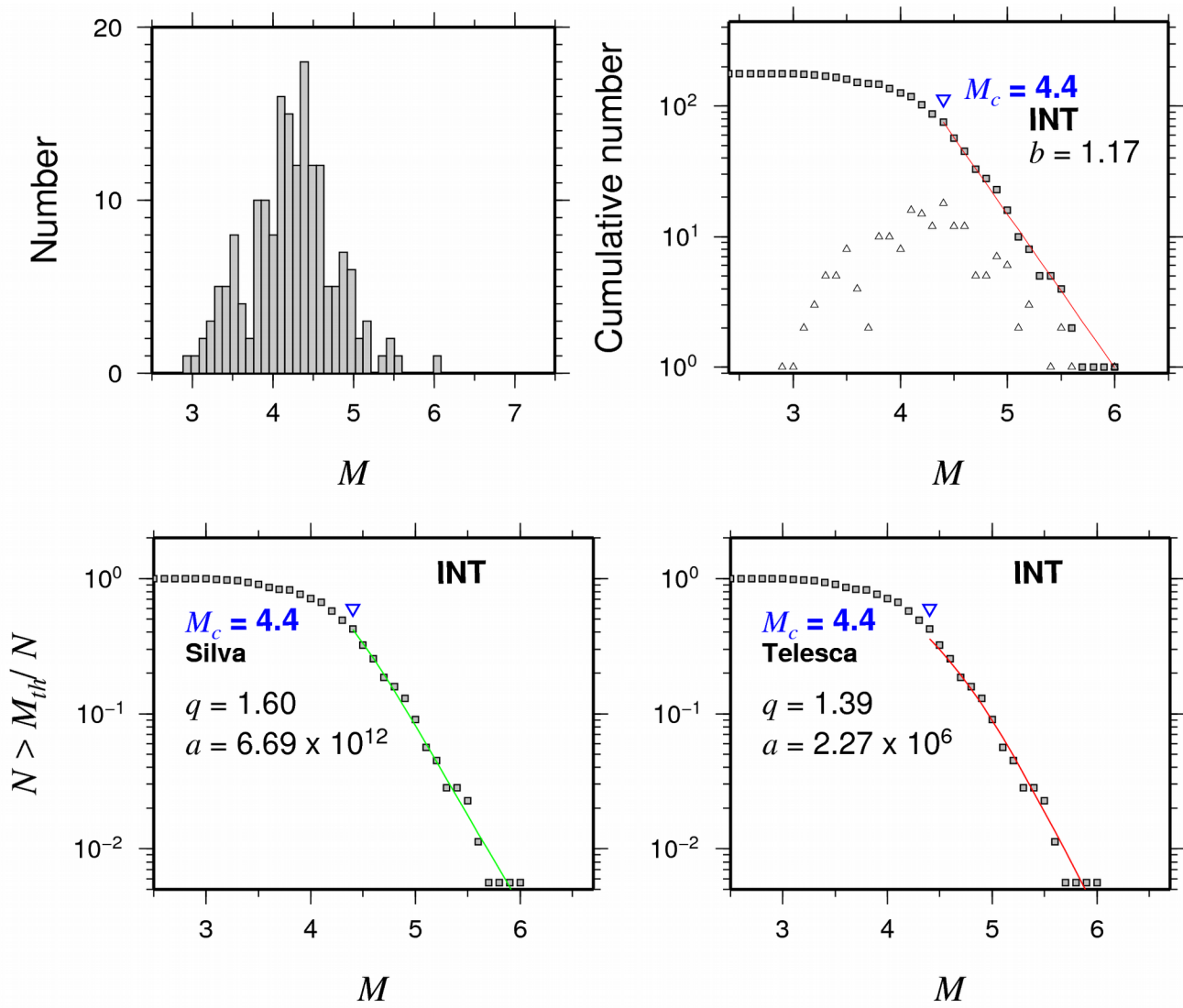
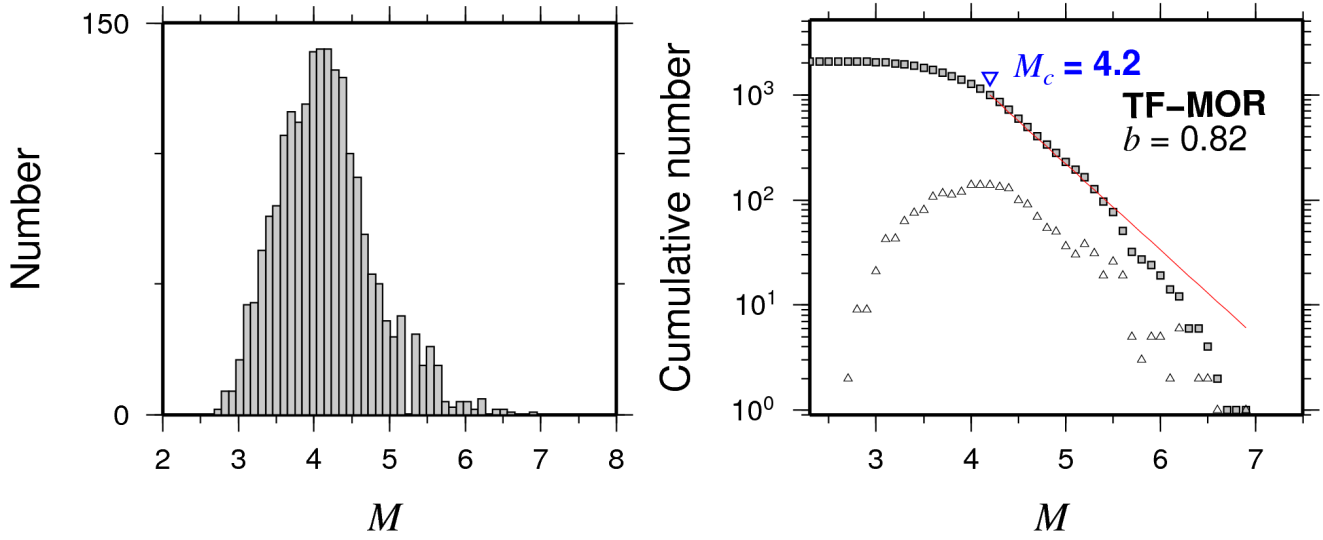


Figure 3

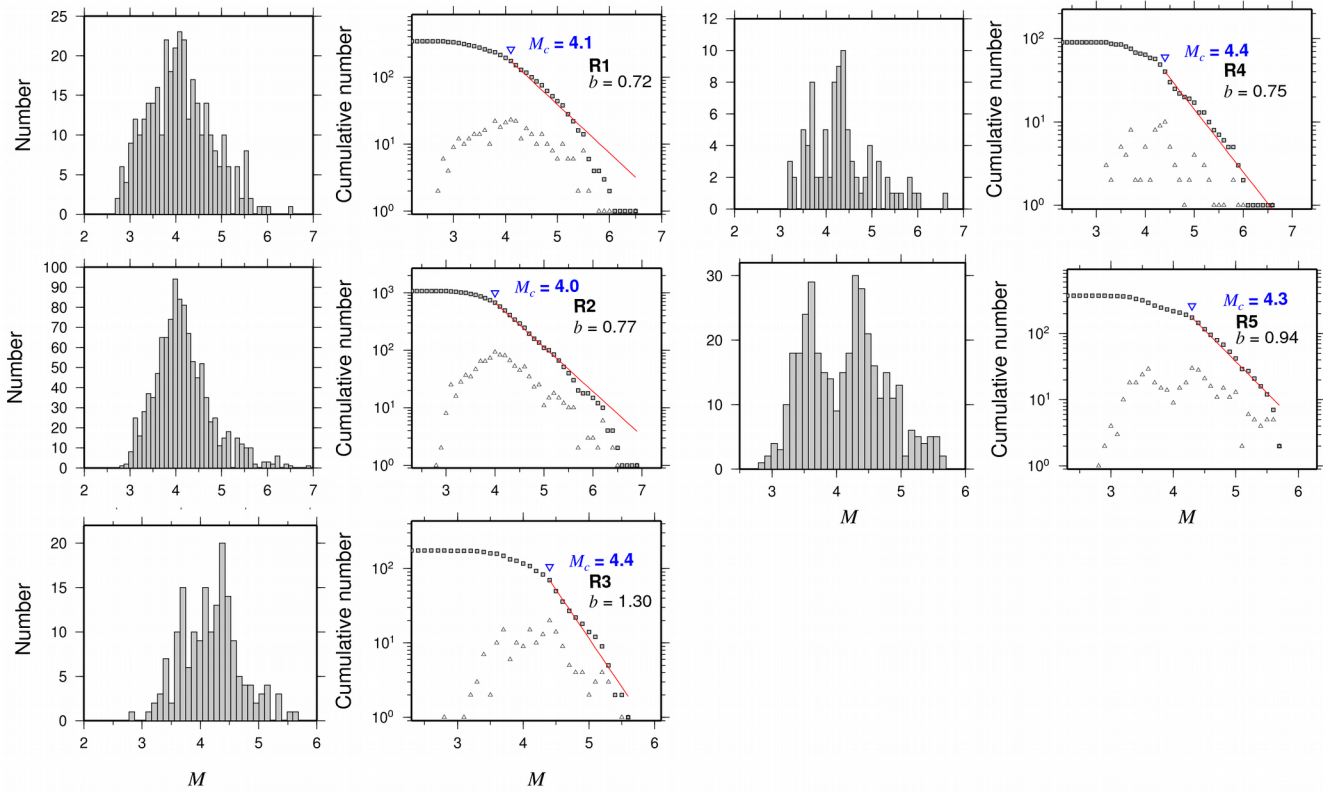
1  
2  
3  
4  
5  
6  
7  
8  
9  
10

1 (a)



2

3 (b)

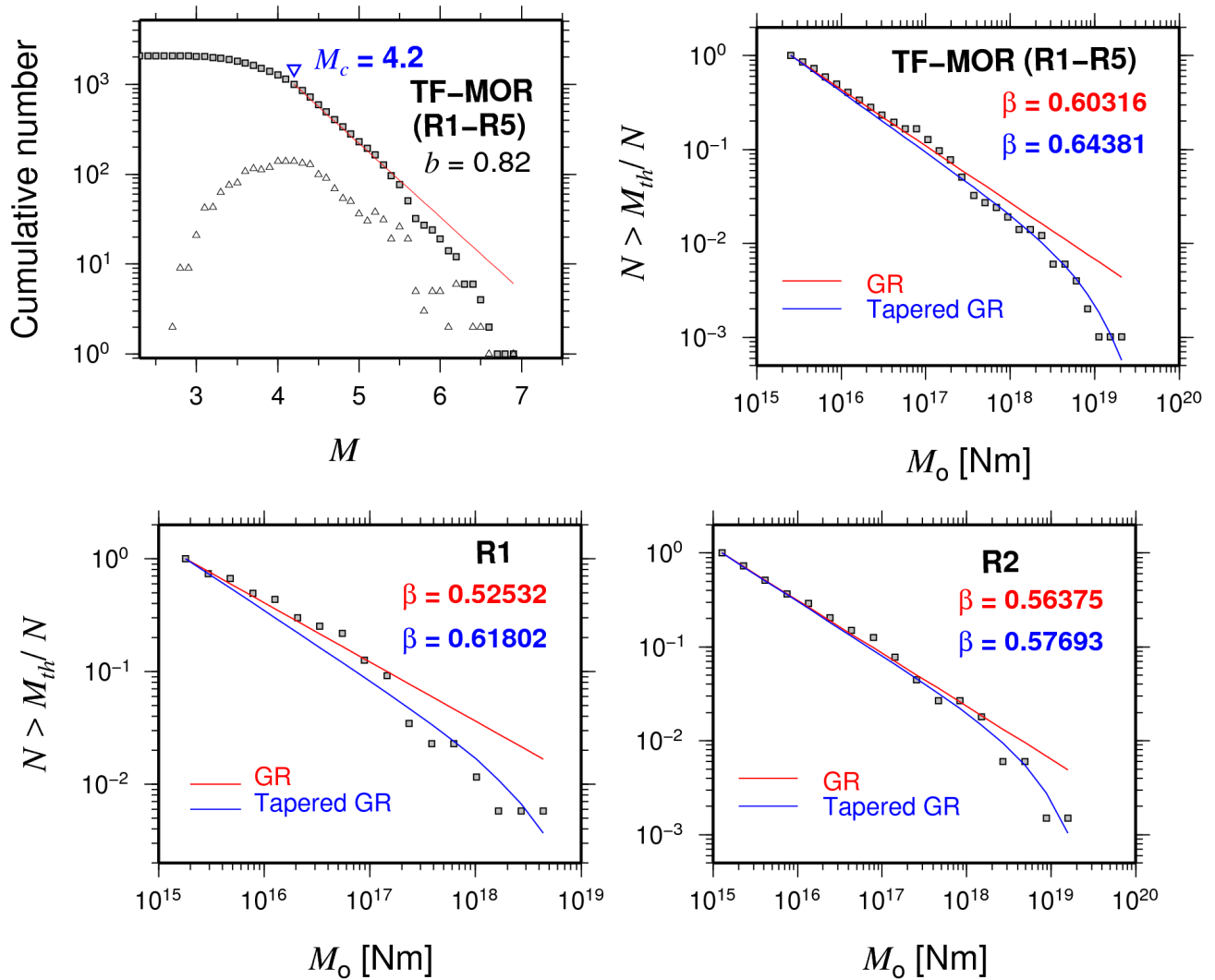


4

5

Figure 4

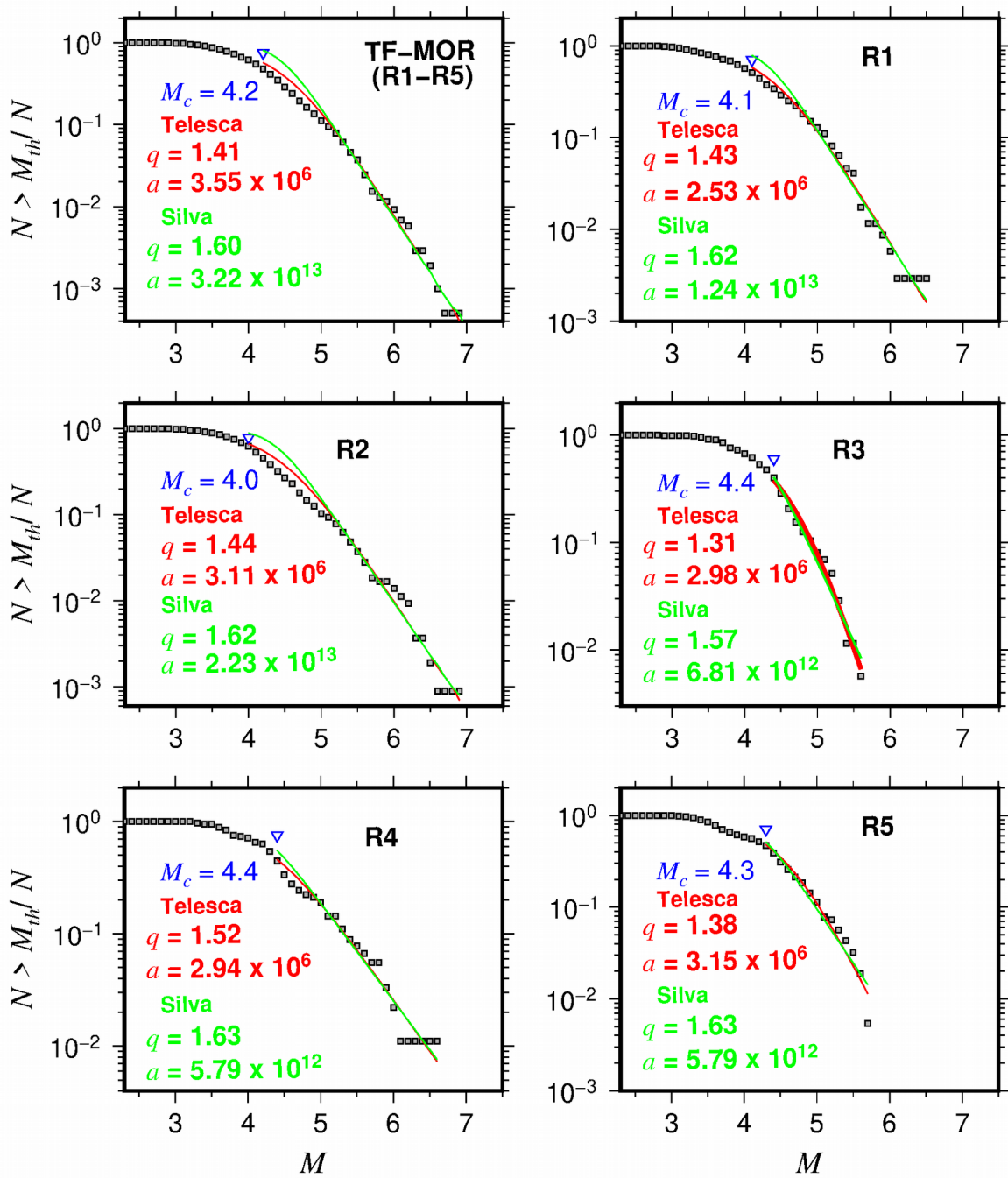
6 Main statistical characteristics for the transform faults zone, and mid-ocean ridges events (TF-MOR)  
 7 (regions R1 to R5) (upper panels). Magnitude earthquake histograms, and frequency magnitude  
 8 distributions with  $M_c$ , and  $b$ -values for each of the different subregions shown in Fig. 8 (lower panels).



1  
2  
3  
4  
5  
6  
7  
8  
9

Figure 5

The cumulative annual seismic moment frequency distribution for the transform faults zone, and mid-ocean ridges events (TF-MOR) (regions R1 to R5) (upper panels). The blue lines are the moment tapered Gutenberg Richter distributions. The red lines represent the ordinary moment Gutenberg Richter distributions. The subregions that do not follow an ordinary moment Gutenberg Richter distribution are subregions R1 and R2 (lower panels).



1

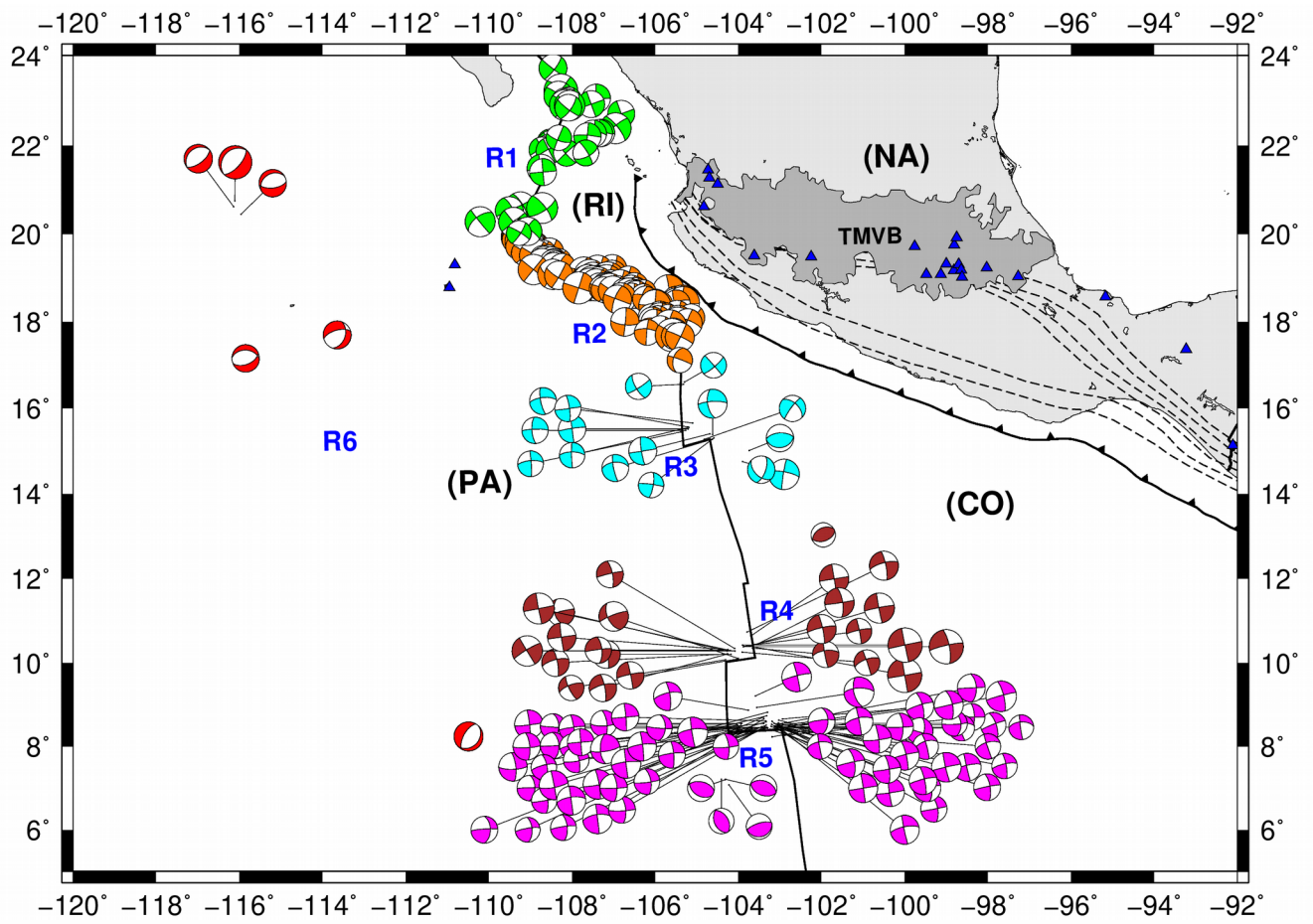
2

Figure 6

3 The normalized cumulative number of events as function of magnitude for the transform faults zone,  
 4 and mid-ocean ridges events (TF-MOR). Blue triangles show the completeness magnitude ( $M_c$ ). Red  
 5 curves show the best fit for the non-extensivity parameters  $q$ , and  $a$  for the Telesca's model (red lines).  
 6 Green curves show the best fit for the non-extensivity parameters  $q$ , and  $a$  for the Silva's model (green  
 7 lines).



1 (a)



2

3

4

5

6

7

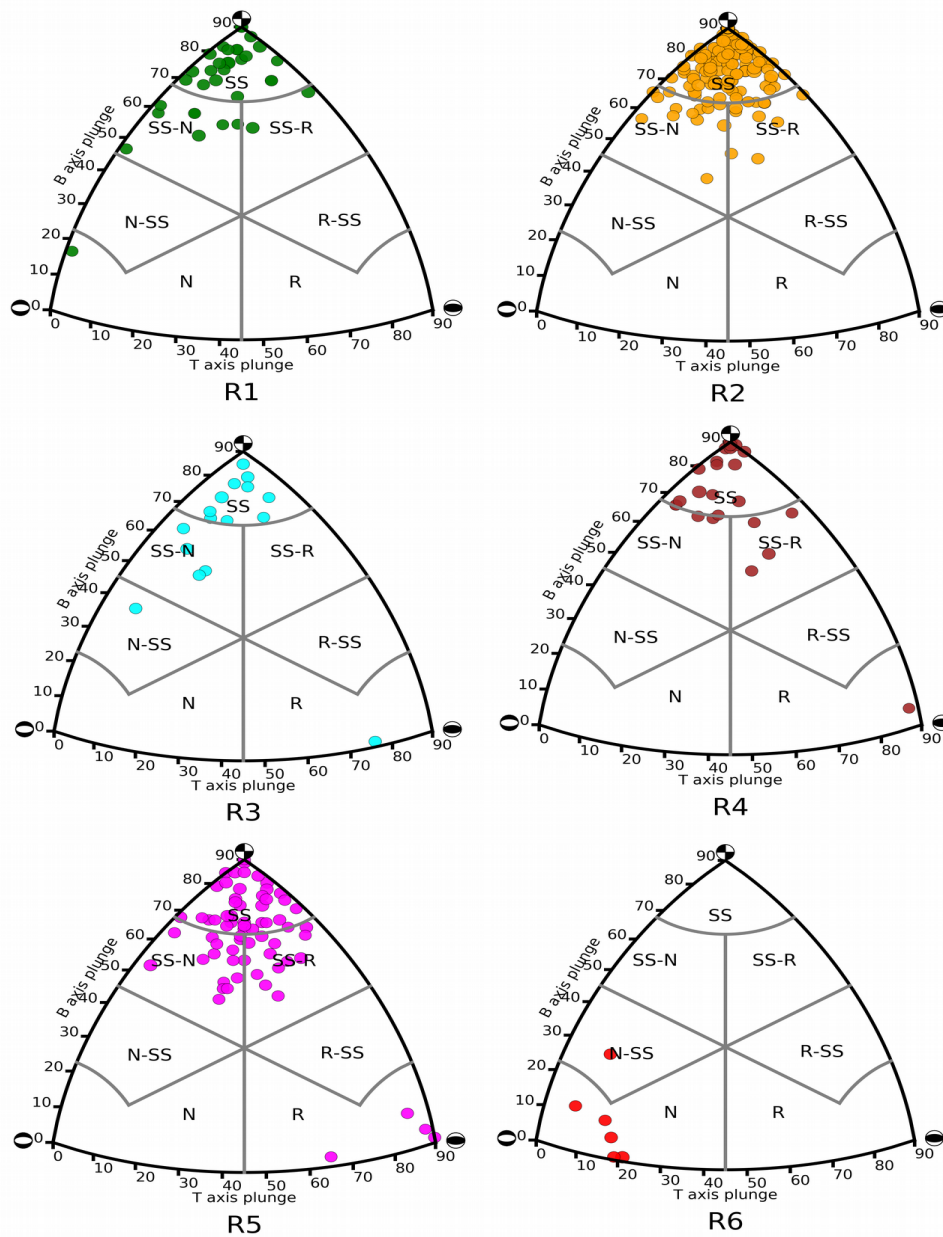
8

9

10

11

1 (b)



2

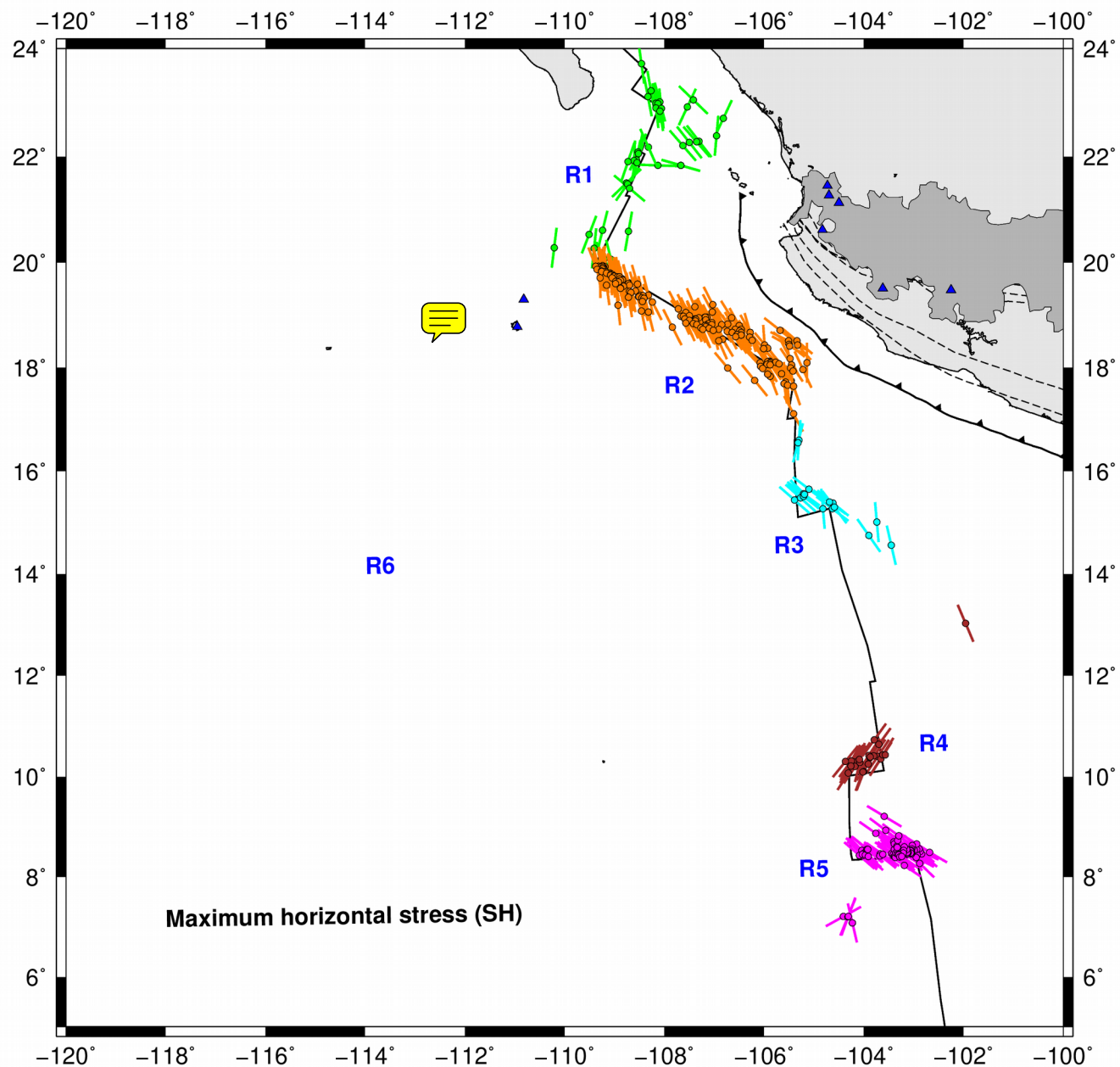
3

Figure 7

4 Focal mechanism solutions of oceanic earthquakes in Mexico reported by the Global CMT catalogue  
5 from 1976 to 2017. a) Focal mechanisms are divided into 6 regions (R1 to R6) for the stress inversion  
6 analysis. b) Focal mechanism classification based on the Kaverina et al. (1996) projection technique  
7 implemented by Álvarez-Gómez (2015): reverse, reverse with lateral component, strike-slip with  
8 reverse component, strike-slip, strike-slip with normal component, normal with lateral component, and  
9 normal (R, R-SS, SS-R, SS, SS-N, N-SS, and N, respectively).



1 (a)



2

3

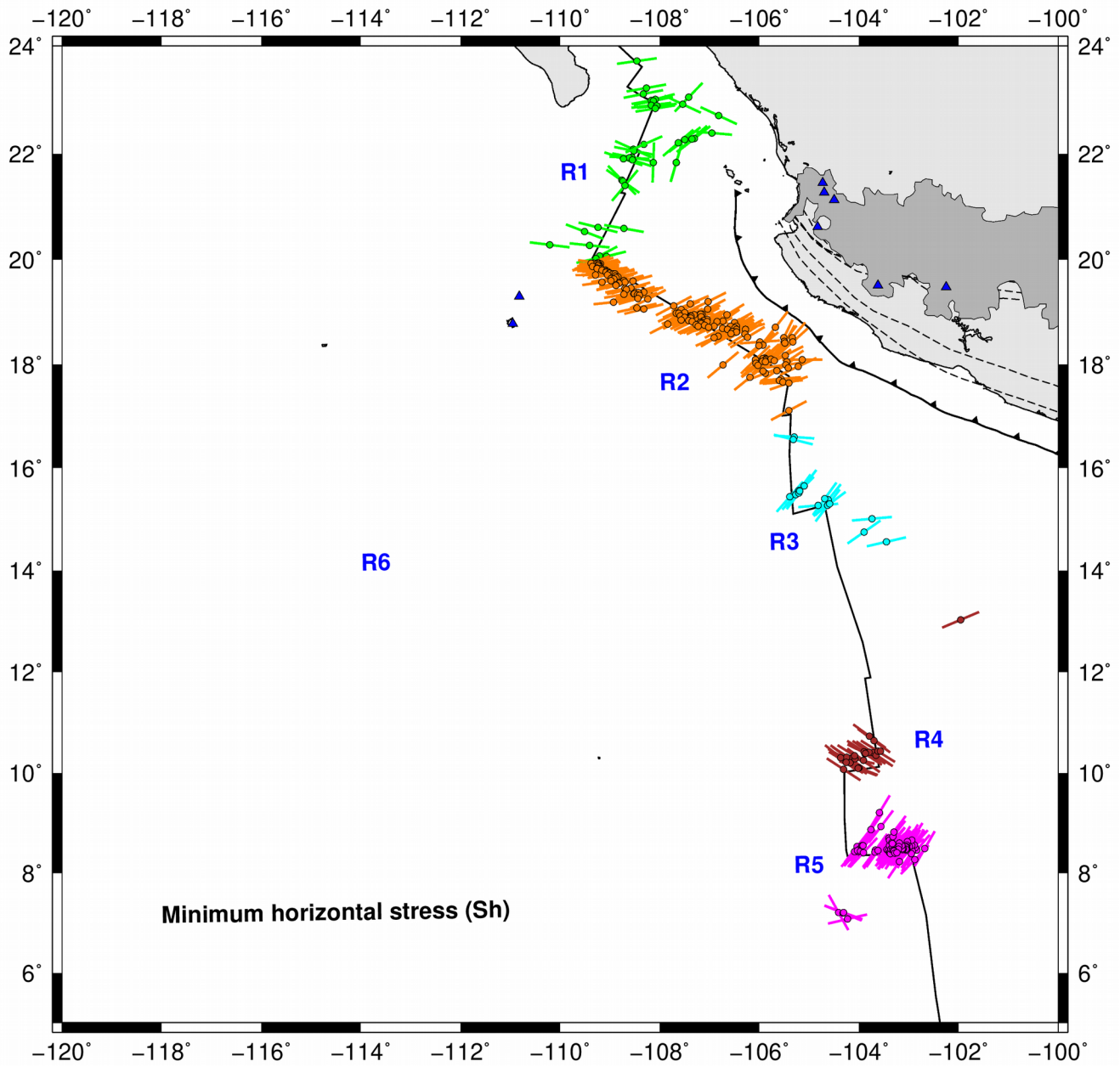
4

5

6

7

1 (b)



2

3

Figure 8

4 Orientation of horizontal axes. a) maximum horizontal stresses (SH); b) minimum horizontal stresses

5 (Sh).

1 **Table 1**

2 Major oceanic earthquakes in Mexico ( $M > 6.8$ )

Event	Date dd/mm/yyyy	Time hh:mm:ss	Lon (°)	Lat (°)	$M_s$	$M_w$	$M_0$	Reference
1	14/01/1899	02:36:00	-110.00	20.00	7.0			1
2	17/12/1905	05:27:00	-113.00	17.00	7.0	7.0	$4.40 \times 10^{19}$	2
3	10/04/1906	21:18:00	-110.00	20.00	7.1	7.1	$6.20 \times 10^{19}$	2
4	31/10/1909	10:18:00	-105.00	8.00	6.9			3
5	31/05/1910	04:54:00	-105.00	10.00	7.0			3
6	29/10/1911	18:09:00	-101.00	11.00	6.8			3
7	16/11/1925	11:54:00	-107.00	18.00	7.0			4
8	28/05/1936	18:49:01	-103.60	10.10	6.8			3
9	30/06/1945	05:31:21	-115.80	16.70	6.8			3
10	04/12/1948	04:00:00	-106.50	22.00	6.9			3
11	29/09/1950	06:32:00	-107.00	19.00	7.0			4
12	01/05/1997	11:37:40	-107.15	18.96	6.8	6.9	$2.77 \times 10^{19}$	5

3 1 Data from the Decade of North American Geology Project (DNA) of the National Geophysical Data  
4 Center (NGDC), and the Geological Society of America.

5 2 Pacheco and Sykes (1992)

6 3 ISC earthquake catalog

7 4 Abe (1981)

8 5 Global CMT catalog

9

10

11

12 **Table 2**

13 Statistical parameters

Type	$M_c$	$b$ -value	$q_s$ -value	$a_s$ -value	$q_T$ -value	$a_T$ -value
INT	4.4	0.89	1.60	$6.69 \times 10^{12}$	1.39	$2.27 \times 10^6$
TF-MOR (R1- R5)	4.1	0.64	1.60	$3.22 \times 10^{13}$	1.41	$3.55 \times 10^6$
R1	4.1	0.72	1.62	$3.22 \times 10^{13}$	1.43	$2.53 \times 10^6$
R2	4.0	0.77	1.62	$1.24 \times 10^{13}$	1.44	$3.11 \times 10^6$
R3	4.4	1.30	1.57	$6.81 \times 10^{12}$	1.31	$2.98 \times 10^6$
R4	4.4	0.75	1.70	$1.12 \times 10^{13}$	1.52	$2.94 \times 10^6$
R5	4.3	0.94	1.63	$5.79 \times 10^{12}$	1.38	$3.15 \times 10^6$

14 INT are intraplate oceanic events; TF-MOR are transform faults zone, and mid-ocean ridges events;  $M_c$   
15 is the completeness magnitude;  $b$  is the slope of the Gutenberg-Richter distribution;  $q_s$ ,  $a_s$ ,  $q_T$ , and  $a_T$   
16 are the non-extensive parameters based on Silva et al. (2006), and Telesca (2011), respectively.

17

18

19

20

21

22

1 **Table 3**

2 Aftershocks characteristics of 1 May 1997 event

Date	$M_m$	$M_a$	$D$	$p$ -value	$c$	$k$
01/05/1997	6.9	5.3	1.6	$0.67 \pm 0.33$	$0.00 \pm 0.53$	$2.12 \pm 1.53$

3  $M_m$  is the magnitude of the mainshock;  $M_a$  is the magnitude of the largest aftershock;  $D$  is the  
 4 difference in magnitudes of the mainshock, and its largest aftershock;  $p$ ,  $c$ , and  $k$  are the coefficients of  
 5 the Omori's law.

6  
7  
8 **Table 4**

9 Stress inversion results

$\sigma_1$ Azimuth/plunge	$\sigma_2$ Azimuth/plunge	$\sigma_3$ Azimuth/plunge	SH <sub>max</sub>	$R$	Region
169°/16°	2°/73°	260°/4°	169	0.37	1 <sup>a</sup>
156°/0°	62°/83°	246°/7°	157	0.58	2 <sup>a</sup>
157°/4°	31°/84°	247°/5°	157	0.63	3 <sup>a</sup>
197°/6°	302°/76°	106°/13°	22	0.84	4 <sup>a</sup>
299°/6°	44°/69°	207°/20°	120	0.73	5 <sup>a</sup>
247°/80°	39°/9°	130°/5°	45	0.73	6 <sup>a</sup>

10 Stress ratio is defined by  $R = (\sigma_1 - \sigma_2) / (\sigma_1 - \sigma_3)$ ; <sup>a</sup>, stress inversion based on Vavryčuk (2014), and  
 11 Lund and Townend (2007). Location of the regions are shown in Fig. 1.

12

13

14

15

16

17

18

19

20

21

22

23

24

1 **Code availability**

2

3 Generic Mapping Tools (GMT5), Available at: <http://gmt.soest.hawaii.edu/>, last access: 13 January  
4 2020.

5

6 Get\_GR\_parameters.m, Available at: <https://jaolive.weebly.com/codes.html>, last access: 23 December  
7 2020.

8

9 FMC, Available at: [https://josealvarezgomez.wordpress.com/2014/04/22/fmc-a-python-program-to-  
10 manage-classify-and-plot-focal-mechanism-data/](https://josealvarezgomez.wordpress.com/2014/04/22/fmc-a-python-program-to-manage-classify-and-plot-focal-mechanism-data/), last access: 13 January 2020.

11

12 Stressinverse\_1.1, Available at: <https://www.ig.cas.cz/en/stress-inverse/>, last access: 13 January 2020.

13

14 ZMAP, Available at: [http://www.seismo.ethz.ch/en/research-and-teaching/products-  
15 software/software/ZMAP/](http://www.seismo.ethz.ch/en/research-and-teaching/products-software/software/ZMAP/), last access: 13 January 2020.

16

17 **Data availability**

18 Earthquake catalogs data available at:

19

20 Earthquake catalog of the Servicio Sismológico Nacional, <http://www.ssn.unam.mx/>, last access: 13  
21 January 2020.

22

23 Earthquake catalog of the International Earthquake Center:

24 <http://www.isc.ac.uk/iscbulletin/search/catalogue/>, last access: 13 January 2020.

1

2 **Team list**

3 Q. Rodríguez-Pérez *E-mail*: [quetza@geociencias.unam.mx](mailto:quetza@geociencias.unam.mx)

4 V.H. Márquez-Ramírez *E-mail*: [marvh@geociencias.unam.mx](mailto:marvh@geociencias.unam.mx)

5 F.R. Zúñiga *E-mail*: [ramon@geociencias.unam.mx](mailto:ramon@geociencias.unam.mx)

6

7 **Author contribution**

8

9 Quetzalcoatl Rodríguez-Pérez, Víctor Hugo Márquez, and Francisco Ramón Zúñiga designed the idea  
10 and discussed the results. Quetzalcoatl Rodríguez-Pérez developed the methodology and performed the  
11 analyses. Quetzalcoatl Rodríguez-Pérez prepared the manuscript with contributions from all co-authors.

12

13 **Competing interests**

14

15 The authors declare that they have no conflict of interest.

16

17

18 *Acknowledgments* We thank the Mexican National Seismological Service (SSN) for providing us with  
19 the earthquake catalog. Station maintenance, data acquisition, and distribution is thanks to its  
20 personnel. Quetzalcoatl Rodríguez-Pérez was supported by the Mexican National Council for Science  
21 and Technology (CONACYT) (Catedras program- project 1126).

22

23

24

## 1 **References**

2

3 Abe, K.: Magnitudes of large shallow earthquakes from 1904 to 1980, *Phys. Earth Planet. Int.*, 27, 72-  
4 92, 1981.

5

6 Abercrombie, R.E., and Ekström, G.: Earthquake slip on oceanic transform faults, *Nature*, 410, 74-77,  
7 2001.

8

9 Abercrombie, R.E., and Ekström, G.: A reassessment of the rupture characteristics of oceanic transform  
10 earthquakes, *J. Geophys. Res.*, 108, B5, 2003.

11

12 Aki, K.: Maximum likelihood estimate of  $b$  in the formula  $\log(N) = a - bM$  and its confidence limits, *B.*  
13 *Earthq. Res. I. Tokyo*, 43, 237-239, 1965.

14

15 Álvarez-Gómez, J.A.: FMC: A program to manage, classify and plot focal mechanism data. Version  
16 1.01, 2015.

17

18 Antolik, M., Abercrombie, R., Pan J., and Ekström, G: Rupture characteristics of the 2003  $M_w$  7.6 mid-  
19 Indian Ocean earthquake: implications for seismic properties of young oceanic lithosphere, *J. Geophys.*  
20 *Res.*, 111, B04302, 2006.

21

22 Bandy, W.L.: Geological and geophysical investigation of the Rivera-Cocos plate boundary:  
23 implications for plate fragmentation, Ph.D. thesis, Texas A&M University, College Station, 195pp.,  
24 1992.

1  
2  
3  
4  
5  
6  
7  
8  
9  
10  
11  
12  
13  
14  
15  
16  
17  
18  
19  
20  
21  
22  
23  
24

Bandy, W.L., Michaud, F., Mortera Gutierrez, C.A., Dymant, J., Bourgois, J., Royer, J.Y., Calmus, T., Sosson, M., and Ortega-Ramirez, J.: The Mid-Rivera-Transform discordance: morphology and tectonic development, *Pure Appl. Geophys.*, 168, 1391-1413, 2011.

Beroza, G.C., and Jordan, T.: Searching for slow and silent earthquakes using free oscillations, *J. Geophys. Res.*, 95, B3, 2485-2510, 1990.

Bird, P., Kagan, Y. Y., and Jackson, D. D.: Plate tectonics and earthquake potential of spreading ridges and oceanic transform faults. In S. Stein and J.T. Freymueller (Eds.), *Plate Boundary Zones, Geodynamics Series*, American Geophysical Union, 203-218, 2002.

Boettcher, M.S., and Jordan, T.H.: Seismic behavior of oceanic transform faults, Fall Meeting, American Geophysical Union (AGU), San Francisco, California, December 10-14, S32E-07, 2001.

Boettcher, M.S., and Jordan, T.H.: Earthquake scaling relations for mid-ocean ridge transform faults, *J. Geophys. Res.*, 109, B12302, 2004.

Boettcher, M.S., Hirth, G., and Evans, B.: Olivine friction at the base of oceanic seismogenic zones, *J. Geophys. Res.*, 112, B01205, 2007.

Boettcher, M.S., and McGuire, J.J.: Scaling relations for seismic cycles on mid-ocean ridge transform faults, *Geophys. Res. Lett.*, 36, L21301, 2009.



- 1 Boettcher, M.S., Wolfson-Schwehr, M.L., Forestall, M., and Jordan, T.H.: Characteristics of oceanic  
2 strike-slip earthquakes differ between plate boundary and intraplate settings, Fall Meeting, American  
3 Geophysical Union (AGU), San Francisco, California, December 3-7, 7245 *Seismology*, 2012.
- 4
- 5 Bohnenstiehl, D.R., Tolstoy, M., Dziak, R.P., Fox, C.G., and Smith, D.K.: Aftershock sequences in the  
6 mid-ocean ridge environment: an analysis using hydroacoustic data, *Tectonophysics*, 354, 49-70, 2002.
- 7
- 8 Bohnenstiehl, D.R., Tolstoy, M., and Chapp, E.: Breaking into the plate: A 7.6  $M_w$  fracture-zone  
9 earthquake adjacent to the central Indian Ridge, *Geophys. Res. Lett.*, 31, L02615, 2004.
- 10
- 11 Bohnenstiehl, D.R., Waldhauser, F., and Tolstoy, M.: Frequency-magnitude distribution of  
12 microearthquakes beneath the 9°50'N region of the East Pacific Rise, October 2003 through April  
13 2004, *Geochem. Geophys. Geosyst.*, 9, Q10T03, 2008.
- 14
- 15 Choy, G.L., and Boatwright, J.: Global patterns of radiated seismic energy and apparent stress, *J.*  
16 *Geophys. Res.*, 100, 18205-18226, 1995.
- 17
- 18 Choy, G.L., and McGarr, A.: Strike-slip earthquakes in the oceanic lithosphere: Observations of  
19 exceptionally high apparent stress, *Geophys. J. Int.*, 100, 18205-18226, 2002.
- 20
- 21 Cowie, P.A., Scholz, C.H., Edwards, M., and Malinverno, A.: Fault strain and seismic coupling on Mid-  
22 Ocean Ridges, *J. Geophys. Res.*, 98, 17911-17920, 1993.
- 23
- 24 Davis, S.D., and Frohlich, C.: Single-link cluster analysis, synthetic earthquake catalogues and

1 aftershock identification, *Geophys. J. Int.*, 104, 289-306, 1991.

2

3 DeMets , C., Gordon, R.G., Argus, D.F., and Stein, S.: Effect of recent revisions to the geomagnetic  
4 reversal time scale on estimate of current plate motions, *Geophys. Res. Lett.*, 21, 2191-2194, 1994.

5

6 Dziewonski, A.M., Chou, T.A., and Woodhouse, J.H.: Determination of earthquake source parameters  
7 from waveform data for studies of global and regional seismicity, *J. Geophys. Res.*, 86, 2825-2852,  
8 1981.

9

10 Ekström, G., Nettles, M., and Dziewonski, A.M.: The global CMT project 2004-2010: centroid-  
11 moment tensors for 13,017 earthquakes, *Phys. Earth Planet. Int.*, 200-201, 1-9, 2012.

12

13 Frohlich, C.: Practical suggestions for assessing rates of seismic-moment release, *B. Seismol. Soc.*  
14 *Am.*, 97, 1158-1166, 2007.

15

16 Gephart, J.W., and Forsyth, D.W.: An improved method for determining the regional stress tensor using  
17 earthquake focal mechanism data: application to the San Fernando earthquake sequence, *J. Geophys.*  
18 *Res.*, 89, 9305-9320, 1984.

19

20 Goslin, J., et al.: Extent of Azores plume influence on the Mid-Atlantic Ridge north of the hotspot,  
21 *Geology*, 27(11), 991-994, 1999.

22

23 Goslin, J., Lourenço, N., Dziak, R.P., Bohnenstiehl, D.R., Haxel, J., and Luis, J.: Long-term seismicity  
24 of the Reykjanes Ridge (North Atlantic) recorded by a regional hydrophone array, *Geophys. J. Int.*,

1 162, 516-524, 2005.

2

3 Gutenberg, B., and Richter, C.F.: Frequency of earthquakes in California, *B. Seismol. Soc. Am.*, 34,  
4 185-188, 1944.

5

6 Houston, H., Anderson, H., Beck., S. L., Zhang, J., and Schwartz, S.: The 1986 Kermadec earthquake  
7 and its relation to plate segmentation, *Pure Appl. Geophys.*, 140, 331-364, 1993.

8

9 Hwang, L.J., and Kanamori, H.: Rupture process of the 1987-1988 Gulf of Alaska earthquake  
10 sequence, *J. Geophys. Res.*, 97, 19881-19908, 1992.

11

12 Ihmlé, P.F., and Jordan, T.H.: Teleseismic search for slow precursors to large earthquakes, *Science*, 266,  
13 1547-1551, 1994.

14

15 Ishimoto, M., and Iida, K.: Observations of earthquakes registered with the microseismograph  
16 constructed recently, *B. Earthq. Res. I. Tokyo*, 17, 443-478, 1939.

17

18 Kagan, Y.Y.: Seismic moment-frequency relation for shallow earthquakes: regional comparisons, *J.*  
19 *Geophys. Res.*, 102, 2835-2852, 1997.

20

21 Kagan, Y.Y.: Universality of the seismic moment-frequency relation, *Pure Appl. Geophys.*, 155, 537-  
22 573, 1999.

23

24 Kagan, Y.Y., and Jackson, D.D.: Probabilistic forecasting of earthquakes, *Geophys. J. Int.*, 143, 438-

1 453, 2000.

2

3 Kagan, Y.Y., and Schoenberg F.: Estimation of the upper cutoff parameter for the tapered pareto  
4 distribution, *J. Appl. Probab.*, 38A, 158-175, 2001.

5

6 Kagan, Y.Y.: Seismic moment distribution revisited: I. Statistical results, *Geophys. J. Int.*, 148, 520-  
7 541, 2002.

8

9 Kagan, Y.Y.: Earthquake size distribution: power-law with exponent  $\beta \equiv 1/2?$ , *Tectonophysics*, 490,  
10 103-114, 2010.

11

12 Kanamori, H., and Stewart, G.S.: Mode of the strain release along the Gibbs fracture zone, Mid-  
13 Atlantic Ridge, *Phys. Earth Planet. Int.*, 11, 312-332, 1976.

14

15 Kaverina, A.N., Lander, A.V., and Prozorov, A.G.: Global creepex distribution and its relation to  
16 earthquake-source geometry and tectonic origin, *Geophys. J. Int.*, 125, 249-265, 1996.

17

18 Kawasaki, I., Kawahara, Y., Takata, I., and Kosugi, I.: Mode of seismic moment release at transform  
19 faults, *Tectonophysics*, 118, 313-327, 1985.

20

21 Kisslinger, C.: Aftershocks and fault-zone properties, *Adv. Geophys.*, 38, 1-36, 1996.

22

23 Klein, F.W., Wright, T., and Nakata, J.: Aftershock decay, productivity, and stress rates in Hawaii:  
24 indicators of temperature and stress from magma sources, *J. Geophys. Res.*, 111(B7), B07307, 2006.

1

2 Läderach, Ch.: Seismicity of ultraslow spreading mid-ocean ridges at local, regional and teleseismic  
3 scales: A case study of contrasting segments, Ph.D thesis, University of Bremen, 116 pp., 2011.

4

5 Lund, B., and Townend, J.: Calculating horizontal stress orientations with full or partial knowledge of  
6 the tectonic stress tensor, *Geophys. J. Int.*, 270, 1328-1335, 2007.

7

8 McGuire, J.J., Ihmlé, P.F., and Jordan, T.H.: Time-domain observations of a slow precursor to the 1994  
9 Romanche transform earthquake, *Science*, 274, 82-85, 1996.

10

11 McGuire, J.J., Boettcher M.S., and Jordan, T.H.: Foreshock sequences and short-term earthquake  
12 predictability on East Pacific Rise transform faults, *Nature*, 434, 457-461, 2005.

13

14 McGuire, J.J.: Seismic cycles and earthquake predictability on East Pacific Rise transform faults, *B.*  
15 *Seismol. Soc. Am.*, 98, 1067-1084, 2008.

16

17 McGuire, J.J., Collins, J.A., Gouédard, P., Roland, E., and Lizarralde, D.: Variations in earthquake  
18 rupture properties along the Gofar transform fault, East Pacific Rise, *Nat. Geosci.*, 5, 336-341, 2012.

19

20 Mogi, K.: Magnitude-frequency relation for elastic shocks accompanying fractures of various materials  
21 and some related problems in earthquakes, *B. Earthq. Res. I. Tokyo*, 40, 831-853, 1962.

22

23 Molchan, G., Kronrod, T., and Panza, G.F.: Multi-scale seismicity model for seismic risk, *B. Seismol.*  
24 *Soc. Am.*, 87, 1220-1229, 1997.

1

2 Nelder, J.A., and Mead, R.: A simplex method for function minimization, *Comput. J.*, 7, 308-313, 1965.

3

4 Nuannin, P., Kulhanek, O., and Persson, L.: Variations of *b*-value preceding large earthquakes in the  
5 Andaman-Sumatra subduction zone, *J. Asian Earth Sci.*, 61, 237-242, 2012.

6

7 Okal, E.A., and Stewart, L.M.: Slow earthquakes along oceanic fracture zones: evidence for  
8 asthenospheric flow away from hotspots?, *Earth Planet. Sci. Lett.*, 57, 75-87, 1992.

9

10 Olive, J-A.: Get\_GR\_parameters.m Matlab function for analysis of earthquake catalogs. Available at:  
11 <https://jaolive.weebly.com/codes.html>, 2016.

12

13 Pacheco, J.F., and Sykes, L.R.: Seismic moment catalog of large shallow earthquakes, 1900 to 1989, *B.*  
14 *Seismol. Soc. Am.*, 82, 1306-1349, 1992.

15

16 Papadakis, G., Vallianatos, F., and Sammonds, P.: Evidence of nonextensive statistical physics behavior  
17 of the Hellenic subduction zone seismicity, *Tectonophysics*, 608, 1037-1048, 2013.

18

19 Pockalny, R.A., Fox, P.J., Fornari, D.J., McDonald, K., and Perfit, M.R.: Tectonic reconstruction of the  
20 Clipperton and Siqueiros Fracture zones: evidence and consequences of plate motion change for the  
21 last 3Myr, *J. Geophys. Res.*, 102, 3167-3181, 1997.

22

23 Rabinowitz, N., and Steinberg, D.M.: Aftershock decay of the three recent strong earthquakes in the  
24 Levant, *B. Seismol. Soc. Am.*, 88, 1580-1587, 1998.

1  
2  
3  
4  
5  
6  
7  
8  
9  
10  
11  
12  
13  
14  
15  
16  
17  
18  
19  
20  
21  
22  
23  
24

Riedesel, M., Orcutt, J.A., McDonald, K.C., and McClain, J.S.: Microearthquakes in the Black Smoker Hydrothermal Field, east Pacific Rise at 21° N, *J. Geophys. Res.*, 87, 10613-10623, 1982.

Rodríguez-Pérez, Q, and Zúñiga, F. R.: Seismicity characterization of the Maravatío-Acambay and Actopan regions, central Mexico, *J. S. Am. Earth Sci.*, 76, 264-275, 2017.

Rodríguez-Pérez, Q, and Zúñiga, F. R.: Imaging *b*-value depth variations within the Cocos and Rivera plates at the Mexican subduction zone, *Tectonophysics*, 734, 33-43, 2018.

Roland, E., Behn, M.D., and Hirth, G.: Thermal-mechanical behavior of oceanic transform faults: Implications for the spatial distribution of seismicity, *Geochem. Geophys. Geosyst.*, 11, Q07001, 2010.

Scholz, C.H.: The frequency-magnitude relation of micro fracturing in rock and its relation to earthquakes, *B. Seismol. Soc. Am.*, 58, 388-415, 1968.

Schorlemmer, D.S., Wiemer, S., and Wyss, M.: Variations in earthquake-size distribution across different stress regimes, *Nature*, 437, 539-542, 2005.

Scordilis, E.M.: Empirical global converting  $M_s$  and  $m_b$  to moment magnitude, *J. Seismol.*, 10, 225-236, 2006.

Shcherbakov, R., Turcotte, D.L., and Rundle, J.B.: A generalized Omori's law for earthquakes aftershocks decay, *Geophys. Res. Lett.*, 31(11), L11613, 2004.

1

2 Silva, R., Franca, G., Vilar, C., and Alcaniz, J.: Nonextensive models for earthquakes, Phys. Rev. E, 73,  
3 026102, 2006.

4

5 Smith, W.D.: The  $b$ -value as an earthquake precursor, Nature, 289, 136-139, 1981.

6

7 Smith, D.K., Tolstoy, M., Fox, C.G., Bohnenstiehl, D.R., Matsumoto, H., and Fowler, M.J.:  
8 Hydroacoustic monitoring of seismicity at the slow-spreading Mid-Atlantic Ridge, Geophys. Res. Lett.,  
9 29(11), 2002.

10

11 Smith, D.K., Escartin, J., Cannat, M., Tolstoy, M., Fox, C.G., Bohnenstiehl, D.R., and Bazin, S.: Spatial  
12 and temporal distribution of seismicity along the northern Mid-Atlantic Ridge ( $15^{\circ}$ - $35^{\circ}$ ), J. Geophys.  
13 Res., 108(B3), 2003.

14

15 Simão, N., Escartín, J., Goslin, J., Haxel, J., Cannat, M., and Dziak, R.: Regional seismicity of the Mid-  
16 Atlantic Ridge: observations from autonomous hydrophone arrays, Geophys. J. Int., 183, 1559-1578,  
17 2010.

18

19 Sotolongo-Costa, O., and Posadas, M.A.: Fragment-asperity interaction model for earthquakes, Phys.  
20 Rev. Lett., 92, 048501, 2004.

21

22 Stein, S., and Pelayo, A.: Seismological constraints on stress in the oceanic lithosphere, Philosophical  
23 Transactions of the Royal Society of London A, 337, 53-72, 1991.

24



- 1 Sykes, L.R.: Mechanism of earthquakes and nature of faulting on the mid-oceanic ridges, *J. Geophys.*  
2 *Res.*, 72, 2131-2153, 1967.
- 3
- 4 Telesca, L.: Nonextensive analysis of seismic sequences, *Physica A*, 389, 1911-1914, 2009.
- 5
- 6 Telesca, L.: A non-extensive approach in investigating the seismicity of L'Aquila area (central Italy),  
7 struck by the 6 April 2009 earthquake ( $M_L = 5.8$ ), *Terra Nova*, 22, 87-93, 2010.
- 8
- 9 Telesca, L.: Tsallis-based nonextensive analysis of the Southern California seismicity, *Entropy*, 13,  
10 1267-1280, 2011.
- 11
- 12 Tolstoy, M., Bohnenstiehl, D.R., and Edwards, M.H.: Seismic character of volcanic activity at the  
13 ultraslow-spreading Gakkel Ridge, *Geology*, 29, 1139-1142, 2001.
- 14
- 15 Tsallis, C.: Possible generalization of Boltzmann-Gibbs statistics, *J. Stat. Phys.*, 52, 479-487, 1988.
- 16
- 17 Urbancic, T.I., Trifu, C.I., Long, J.M., and Young, R.P.: Space-time correlation of  $b$ -values with stress  
18 release, *Pure Appl. Geophys.*, 139, 449-462, 1992.
- 19
- 20 Utsu, T.: A statistical study on the occurrence of aftershocks, *Geophysical Magazine*, 30, 521-605,  
21 1961.
- 22
- 23 Utsu, T., Ogata, Y., and Mutsaers, R.S.: The centenary of the Omori formula for a decay law of  
24 aftershock activity, *J. Phys. Earth.*, 43, 1-33, 1995.

1

2 Utsu, T.: Statistical features of seismicity, International Handbook of Earthquake and Engineering  
3 Seismology, Part A. Academic Press, pp. 719-732, 2002.

4

5 Valverde-Esparza, S.M., Ramirez-Rojas, A., Flores-Marquez, E.L., and Telesca, L.: Non-extensivity  
6 analysis of seismicity within four subduction regions in Mexico, Acta Geophys., 60, 833–845, 2012.

7

8 Vavryčuk, V.: Iterative joint inversion for stress and fault orientations from focal mechanisms,  
9 Geophys. J. Int., 199, 69-77, 2014.

10

11 Velasco, A.A., Ammon, C.J., and Beck, S.L.: Broadband source modeling of the November 8, 1997,  
12 Tibet ( $M_w = 7.5$ ) earthquake and its tectonic implications, J. Geophys. Res., 105(B12), 28065-28080,  
13 2000.

14

15 Vere-Jones, D., Robinson, R., and Yang, W.Z.: Remarks on the accelerated moment release model:  
16 problems of model formulation, simulation and estimation, Geophys. J. Int., 144, 517-531, 2001.

17

18 Vilar, C.S., Franca, G., Silva, R., and Alcaniz, J.S.: Nonextensivity in geological faults?, Physica A,  
19 377, 285-290, 2007.

20

21 Vallianatos, F.: A non-extensive approach to risk assessment, Nat. Hazards Earth Syst. Sci., 9, 211-216,  
22 2009.

23

24 Warren, N.W., and Latham, G.V.: An experimental study of the thermally induced microfracturing and

1 its relation to volcanic seismicity, J. Geophys. Res., 75, 4455-4464, 1970.

2

3 Wesnousky, S.G.: The Gutenberg-Richter or characteristic earthquake distribution, which is it?, B.

4 Seismol. Soc. Am., 84, 1940-1959, 1994.

5

6 Wiens, D.A., and Stein, S.: Intraplate seismicity and stresses in young oceanic lithosphere, J. Geophys.

7 Res., 89, 11442-11464., 1984.

8

9 Wiemer, S., and Benoit, J.P.: Mapping the *b*-value anomaly at 100 km depth in the Alaska and New

10 Zealand subduction zones, Geophys. Res. Lett., 23, 1557-1560, 1996.

11

12 Wiemer, S., and Wyss, M.: Minimum magnitude of completeness in earthquake catalogues: Examples

13 from Alaska, the western United States, and Japan, B. Seismol. Soc. Am., 90, 859-869, 2000.

14

15 Wiemer, S.: A software package to analyze seismicity: ZMAP, Seismol. Res. Lett., 72, 373-382, 2001.

16

17 Wolfe, C.J., Bergman, E.A., and Solomon, S.C.: Oceanic transform earthquakes with unusual

18 mechanisms or locations: relation to fault geometry and state of stress in the adjacent lithosphere, J.

19 Geophys. Res., 98, B9, 16187-16211, 1993.

20

21 Wolfson-Schwehr, M., Boettcher, M.S., McGuire, J.J., and Collins, J.A.: The relationship between

22 seismicity and fault structure on the Discovery transform fault, East Pacific Rise, Geochem. Geophys.

23 Geosyst., 15, 3698-3712, 2014.

24

- 1 Wyss, M.: Towards a physical understanding of the earthquake frequency distribution, *Geophys. J. Roy. Astron. Soc.*, 31, 341-359, 1973.
- 2